FABRICATION AND CHARACTERIZATION OF MULTIFUNCTIONAL PARTICLES WITH SPATIALLY SEGREGATED PROTEINS

A Thesis
Presented to
The Academic Faculty

by

Kathryn Elizabeth Murray

In Partial Fulfillment
of the Requirements for the Degree
Master of Science in Biomedical Engineering

Georgia Institute of Technology
Emory University

December 2017

FABRICATION AND CHARACTERIZATION OF MULTIFUNCTIONAL PARTICLES WITH SPATIALLY SEGREGATED PROTEINS

Approved by:

Dr. Todd Sulchek, Advisor
School of Mechanical Engineering
Georgia Institute of Technology

Dr. Ravi Kane
School of Chemical and Biomolecular Engineering
Georgia Institute of Technology

Dr. Julie Champion
School of Chemical and Biomolecular Engineering
Georgia Institute of Technology

Date Approved: August 15, 2017

ACKNOWLEDGEMENTS

I would like to thank my advisor, Dr. Todd Sulchek, for his support, guidance, and belief in me on this project and my graduate career journey. Thanks to my committee members, Dr. Ravi Kane and Dr. Julie Champion, for their support and critiques. My fellow colleagues in the Sulchek BioMEMS and Biomechanics Laboratory have been an amazing support system for me, and they provided me with technical and emotional support.

Additionally, I would like to thank my peers, and most of all, my friends whom have shared tears of joy and of frustration throughout this whole process. They believed in me and encouraged me at every moment.

Finally, I would like to thank my parents who have been there for me for all the good times and bad times, and whether they understood my research or not.

.

TABLE OF CONTENTS

LIST OF TABLES

LIST OF FIGURES

LIST OF ABBREVIATIONS

Al	Aluminum
APC	Allophycocyanin
APTES	(3-Aminopropyl)triethoxysilane
Au	Gold
Cu	Copper
DAPI	4',6-Diamidino-2-Phenylindole
diH_2O	Deionized water
EDS	Energy dispersive x-ray spectroscopy
FITC	Fluorescein isothiocyanate
GFP	Green fluorescent protein
HIS	Histidine
IEN	Institute for Electronics and Nanotechnology
IgG	Immunoglobulin G
IL6	Interleukin 6
IMAC	Immobilized metal affinity chromatography
MSC	Mesenchymal stem cell
NF	Non-functionalized
Ni	Nickel
NTA	Nitrilotriacetic acid
PEG	Polyethylene glycol
SA	Streptavidin
SEM	Scanning electron microscopy

SiO_2	Silica
SPBCL	Scanning-probe block copolymer lithography
TPB	Thiol-PEG-biotin
VEGF	Vascular endothelial growth factor
XPS	X-ray photoelectron spectroscopy

SUMMARY

Multifunctional particles have been of great interest in a variety of fields including electronics, biology, chemistry, and medicine due to their ability to have multiple functionalities, both biological and non-biological, in a single entity. In therapeutic design, they have the potential to simultaneously target a specific site, monitor delivery as well as carry multiple drugs. Despite the many advances in multifunctional particles, there are still few methodologies that can spatially control multiple chemical and biological ligands on a single particle. In this thesis, a novel method has been explored to fabricate multi-sided particles using repeated glancing angle metal evaporation on microparticles and nanoparticles. We further showed that this method can enable spatial segregation of proteins on individual particles. Through this investigation, the order of functionalization and thickness of metal evaporation layer were found to be important variables in achieving spatial segregation of the functionalized protein. Additionally, these particles can be imbued with other non-biological and unique functionalities based on choice of metal, such as magnetic and antimicrobial properties, which have been preliminarily explored. Overall, this work demonstrates a novel methodology for the creation of a spatially patterned particles which can be made to be multifunctional and reconfigurable, for a variety of potential applications.

CHAPTER 1 INTRODUCTION

1.1 Background and Significance

Multifunctional particles have been of great interest in many fields due to their ability to have multiple functionalities, both biological and non-biological, in a single entity. In therapeutic design, they have the potential to simultaneously target a specific site, monitor delivery as well as activate multiple therapeutic pathways at once. Often called "designer particles," the functionalities and conjugated moieties of these particles can be tailored to specific applications and therapeutic aims[1,2]. Some of the many applications include catalysis, plasmonics, magnetics, electronics, biology, and medicine[3,4,5,6,7].

There are many reviews on fabrication and applications of multifunctional particles[7,8,9,10]. A majority of these systems employ a combination of polymeric and hydrogel multicomponent systems in order to encapsulate multiple growth factors[11,12,13,14]. Other methods include layered electrospinning of different polymers[15] and passive adsorption[16,17,18,19,20] in order to create multifunctional particles. Non-polymer based particles are often gold nanoparticles that possess additional unique electrochemical properties. For most of these techniques, the multifunctional particles have limited spatial control of the conjugated ligands or functionalities[21,16].

Despite the many advances in multifunctional particles, there are still very few methodologies to spatially control multiple chemical and biological ligands on individual particles. There is a well-established literature describing dual ligand spatial control, referred to as Janus particles. Janus particles are a type of particle that has two chemically

distinct hemispheres. The name comes from the Roman god, Janus, who had two faces on his head. This asymmetry allows for spatial separation of ligands onto individual sides, combinations of typically incompatible substances, and directionality[13]. In addition to having the ability for molecules to be encapsulated, molecules can be attached to the surface of the particle. One application for this is cell specific targeting in vivo[22]. These targeting moieties must be presented on the surface of the particle for binding to the target. Additionally, if the particle is used as a monitoring system, the marker must be accessible to visualization[17].

Some prior demonstrated methods to make spatially segregated particles include microcontact printing method[2], microfluidic fabrication of multicomponent systems[10,23], co-jetting[11,14], and Pickering emulsion[24]. Rahmani et al. developed chemically orthogonal three-patch microparticles which uses a co-jetting process with synthetic polymer chemistry to create particles on the 10-15 μm range[14]. Prior to co-jetting, the polymers are functionalized with polylactide derivatives. Despite the ability to produce uniform particles, co-jetting methods have an inherent geometrical size limitation of the produced particles based on tip size. Additionally, multifunctional particles made through encapsulation/release systems have a wide range of sizes from the millimeter range[15] to hundreds of microns[25].

In exploring techniques to create non-polymeric multifunctional particles, there are two main methods used. The first method is called scanning-probe block copolymer lithography (SPBCL), which is a method which synthesizes polyelemental particles of multiple metals and the spatial segregation of the metals is based on the miscibility of the metals used. Chen *et al.* expanded this synthesis process to up to 5 metals resulting in

particles that are tunable based on the ratio of metal content present in the ink solution[26]. While the diameters of these particles are around 40 nm, the process takes a minimum of 60 hours and must be performed at high temperatures. Yield and efficiency is also a concern for this fabrication method.

Prior work has also developed Janus particles using a metal evaporation technique to coat a single hemisphere of both silica and polystyrene particles with gold[27]. In this work, it was shown that using silica particles produces high yield and fabricated with high uniformity. The methods established provide spatial segregation of the protein conjugated to each surface, with the silica base hemisphere modified with APTES and the gold hemisphere modified with a thiol-PEG-biotin (TPB) linker to Streptavidin (SA). It is noted that, using e-beam evaporation is highly directional due to the mean free path of evaporated species and therefore coats only the top side of the sample creating a surface modified region for which individual regions can be functionalized. Metal evaporation has the potential to produce nanometer sized particles, more than 2 regions, and customizable chemically distinct surface regions.

While the field has explored a variety of methods mentioned previously, there remains an inability to create multi-region particles which can independently be functionalized to create spatial separation of ligands. Additionally, a method that is compatible with a variety of particle sizes down to 100 nm would benefit therapeutic applications.

1.2 **Objectives**

The objective of this thesis is to develop a general methodology to fabricate novel, multi-sided Cerberus particles using metal evaporation which can allow for spatially segregated proteins on each region. Additionally, we will develop a methodology for creating trifunctional Cerberus particles and explore magnetic forward and rotational targeting.

1.3 **Hypothesis**

Based on the objective above, we hypothesize that repeated metal evaporations at different glancing angles can provide a substrate upon microparticles which regions can be distinctly functionalized with protein.

CHAPTER 2 MATERIALS AND PARTICLE METHODS

In this thesis, multi-sided particles were developed and characterized. First a method for spatially modifying the surface composition of microparticles and nanoparticles. Second, an optimal functionalization procedure was tested to create of a three-sided 'Cerberus' particle with different proteins to each side, creating a spatially segregated trifunctional, biologically active particle. While there have been many developments of multifunctional particles and multi-compartmental capsules, there are no methods that describe spatially segregated, three or more multifunctional particles. Additionally, the methods to create these types of particles are time consuming, using high temperature processes, and often trade spatial separation of protein for functionality, or vice versa. Thus, through the development of trifunctional Cerberus particles, we also explore the use of repeated glancing angle metal evaporation as a means of fabricating particles with multiple chemically distinct regions of different sizes. The following methods describe a generalized protocol used in optimizing a methodology to develop multi-region particles and functionalize three-region Cerberus particles with spatial segregation, with details described in Chapter 3.

Silica particles (diameter = 4, 1, 0.15 μm) were purchased from Bangs Laboratories Inc. (Fishers, IN). (3-Aminopropyl)triethoxysilane (APTES), rabbit immunoglobulin G (rIgG) antibody, nonfat-dried milk bovine, and BSA were purchased from Sigma-Aldrich (St. Louis, MO). Alexa Fluor 488 conjugated goat anti-rabbit IgG, Alexa Fluor 647 conjugated with streptavidin (SA), phosphate-buffered saline (PBS) were purchased from Invitrogen (Carlsbad, CA). Thiol-poly(ethylene glycol)-biotin was purchased from Nanocs

(New York, NY). Ethanol, acetone, and other chemicals were purchased and used as received from VWR (Radnor, Pennsylvania). Lightning-Link Streptavidin kit, 10 and 100ug kits, were purchased from Innova Biosciences. GFP Tag Antibody, mouse, GFP Recombinant Aequorea victoria Protein, N-His Tag, was purchased from ThermoFisher. Kapton polyimide tape and aluminum bar was purchased from McMaster Carr.

2.1 Particle preparation

Silica (SiO_2) particles, 4 μm, 1 μm, and 0.15 μm diameter, were washed to remove surfactants and prepared in a dispersive layer in order to allow all sides of the particle to be accessible during the metal evaporation process. All washing steps involved first centrifugation to pellet the particles, removal of supernatant, and resuspension of pellet of particles in diH_2O, PBS, or EtOH. For particle preparation on glass slides, particles were resuspended in 50% EtOH during the first wash and in 100% EtOH during the second wash. The particles were diluted to a final concentration that would minimize clustering of particles when dried onto glass slides. For 4 μm particles, the concentration of the particles used was $5.2x10^7$ particles/mL. Glass slides were cleaned prior to particles being spotted onto the surface in diH_2O in a sonicator. Cleaned particles were spotted onto the cleaned glass slides using 2-3 μL droplets and dried at room temperature.

2.2 Fabrication of patterned particles through metal evaporation

A microfabrication shadowing technique was used to create multiple chemically-distinct regions on the dispersed, dried silica particles on glass. Deposition of layers of gold and nickel using metal evaporation (Denton Explorer and CHA-2 e-beam evaporator) onto the dispersive layer of particles at two different glancing angles allows uniform and equal

coatings. The angles assessed were 60°, 45°, 30°, 0° and the same angles on the opposition direction of the glass slides (-60°, -45°, -30°). Metal evaporation results in a unidirectional flux of metal deposition that permanently masks only the exposed hemisphere. The opposing hemisphere is shielded from the metal deposition and remains unchanged. Glass slides are attached to one side of the angled sample holder which is then placed inside evaporator. The evaporator is evacuated to a pressure of at least $1x10^{-5}$ Torr to allow for a high mean free path. Then, the first metal is deposited following the instruction for each evaporation machine. Deposition rate was typically 2 A/s. Following the first metal, the glass slides were removed from the evaporator, physically rotated 90 degrees on the slide holder, and placed back into the evaporator for the second metal deposition. The metals successfully evaporated onto particle surfaces included gold, nickel, copper, titanium, and aluminium. For gold deposition layers, a thin titanium adhesion layer of 5 nm must be performed first while the other metals do not require an adhesion layer. The metal thicknesses tested ranged from 20 nm to 100 nm, and all metal layers in a single fabrication batch was the same thickness. The general process is depicted in Figure 2-1.

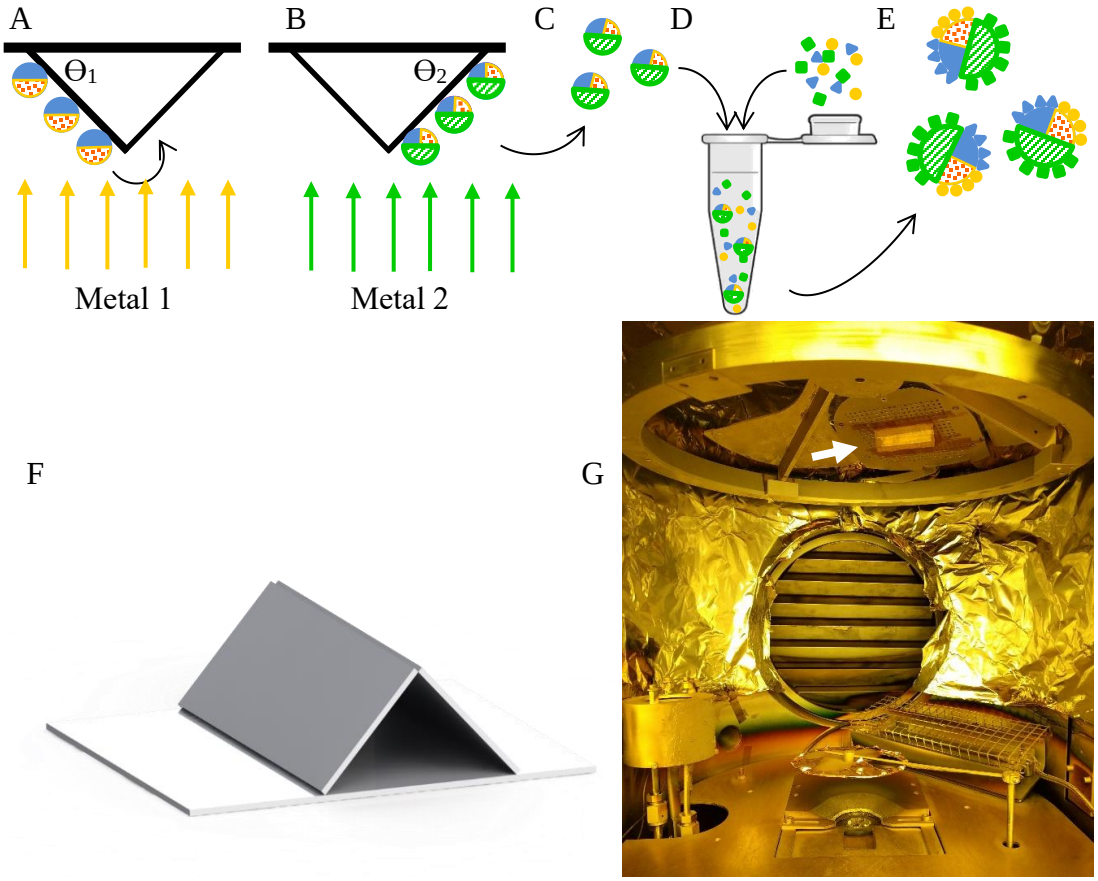

Figure 2-1. Fabrication and functionalization of Cerberus particles. (A) Metal evaporation with metal 1 (orange, speckled) followed by a rotation and (B) second metal evaporation of metal 2 (green, striped) at two distinct angles (θ_1, θ_2) coat the particles creating (C) three chemically distinct regions which are removed from the surface and then (D) functionalized with different proteins via various conjugation schemes. (E) Trifunctional Cerberus particles. (F) Angled slide holder design used to create specifically oriented metal regions on the particles. (G) Image of one of the e-beam metal evaporators with a slide holder and particles, white arrow.

After the metal deposition at two glancing angles, approximately 200 µL diH_2O was spotted on the particles on each glass slide and a cell scraper was used to remove the metal coated Cerberus particles. For each batch created, 15-26 slides of particles were used, thus the particles were in ~5 mL total. The particles were then concentrated to a volume of ~1.5 mL via centrifugation and the concentration was determined through both flow cytometry and hemocytometer analysis. Verification of metal deposition and spatial patterning was

performed with SEM (Zeiss Ultra60 FE-SEM and Hitachi SU8230), with additional elemental analysis performed with EDS (Aztec software).

2.3 Cerberus particle functionalization process through protein conjugation

After verification of metal deposition coating and creation of multiple chemically distinct regions, one subset of the fabricated particles were functionalized. Particles with three regions consisting of gold, nickel, and silica were then functionalized with three different proteins. In order to functionalize each of the three chemically distinct regions of the Cerberus particle, functionalization order was optimized in order to achieve spatial segregation of the different proteins. Silica particles with gold and nickel evaporated at two different glancing angles were conjugated with these general conjugation chemistries. On the silica side of the particles, APTES was used to activate the -OH groups and bind IgG which was subsequently labeled with a primary antibody and a secondary antibody in DAPI. To functionalize the gold side, the Cerberus particles were incubated with thiol-PEG-biotin followed by APC-labeled Streptavidin (SA). Finally, HIS-tagged recombinant green fluorescent protein (GFP) was conjugated to the nickel. Details of the optimization and final protocol are described and assessed in Chapter 3.

2.3.1 APTES

Previous work done resulted in a well-defined method for (3-Aminopropyl)triethoxysilane (APTES) treatment and subsequent protein conjugation to plain silica particles[27]. APTES is a silane coupling agent that activates exposed hydroxyl groups on a surface to allow protein adsorption. Briefly, the Cerberus particles were washed in ethanol, followed by a 2% APTES treatment in ethanol for 2 minutes. The

particles were centrifuged, the supernatant was aspirated, and the particles were resuspended in diH_2O to remove any unreacted APTES. Due to APTES being a non-specific and non-covalent conjugation method, the protein intended for conjugation to the silica region was incubated individually with the particles immediately subsequent to the APTES treatment.

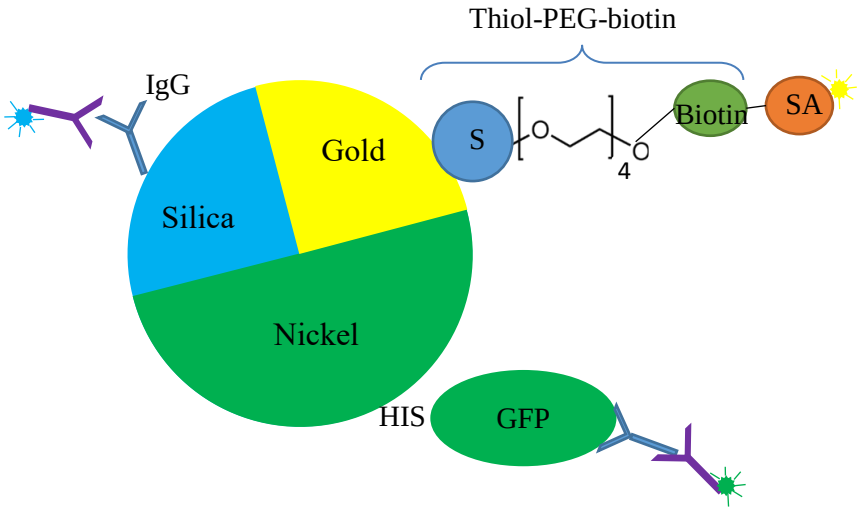

Figure 2-2. General schematic for conjugation schemes for functionalization of three-region Au, Ni, and silica Cerberus particles. Silica is activated with APTES and IgG is conjugated to the activated silica. Thiol-PEG-biotin binds to the gold through thiol-gold interactions. Streptavidin (SA) then binds biotin. HIS-GFP binds nickel and is fluorescently labeled.

2.3.2 Thiol-PEG-Biotin

Thiol-poly(ethylene glycol)-biotin (TPB) is a bifunctional spacer molecule, providing a thiol group, which has a high affinity for gold and a biotin group, which has a high affinity and selectivity for streptavidin (SA). The gold-thiol interaction is frequently used and forms Au-sulfur bonds[28]. On the exposed side, the biotin provides a small, stable, and highly selective molecule for which streptavidin and streptavidin-labeled protein can bind [9]. This high specificity and selectivity makes it an ideal system for multifunctional

and spatially patterning of particles. In this study, the gold-nickel-coated Cerberus particles were incubated in a 0.5 mM TPB solution for 4 hours, followed by a wash cycle in PBS before further processing and functionalization.

2.3.3 Histidine tag

Histidine residues are known to have a strong interaction with metal ions through chelation. This method is used in immobilized metal affinity chromatography (IMAC) which was developed in the 1970s with the advent of recombinant technology[29]. Recombinant proteins can be produced to contain typically 6 histidine residues at either the C- or N-terminus which will bind to nickel. In order to functionalize the nickel side of the Cerberus particles, 6.25 μg/μL histidine-tagged protein, green fluorescent protein (GFP) in this study, was incubated with the particles for 1-2 hour at room temperature. The particles were then washed with PBS to remove excess protein.

2.4 **Particle analysis**

2.4.1 SEM and EDS

After the fabrication of these multi-region Cerberus particles, they were characterized by scanning electron microscopy (SEM) and energy-dispersive x-ray spectroscopy (EDS) using the facilities in the Georgia Tech Institute for Electronics and Nanotechnology (IEN) Materials Characterization Facility. Confirmation and analysis of the metal deposition was performed with the Hitachi SU8239 SEM and Zeiss Ultra 60 FE-SEM. These systems are both equipped with EDS capabilities and Aztec software for elemental analysis. These characterizations were performed after metal deposition but

before removal from the glass slides as well as after the particles were removed from the glass slides to ensure the deposited metal did not flake off the particles.

2.4.2 Flow cytometry and fluorescent microscopy

Flow cytometry was performed using a BD LSR Fortessa with FACSDiva, and data were analysed with FlowJo (TreeStar, Inc.) in order to determine the intensity distribution of the fluorescence for each fluorescently-labeled protein to verify functionalization of a population of at least 10,000 particles. Proteins conjugated to the silica, gold, and nickel regions were stained with AlexaFluor 405 (IgG), APC (Streptavidin), and AlexaFluor 488 (GFP), respectively. Debris was identified and gated out using forward and side scatter. Control groups consisted of non-functionalized Cerberus particles and single-side conjugated Cerberus particles (405/IgG only, APC/Streptavidin only, and 488/GFP only). The single stained controls were used for compensation and gating in FlowJo. Additionally, fluorescent microscopy was used to verify both functionalization and spatial segregation of the three proteins onto the fabricated particles (PerkinElmer UltraVIEW). Brightfield images were also taken and all images were analysed using Volocity (PerkinElmer).

2.5 **Magnetic analysis**

In order to evaluate the magnetic properties of the Cerberus particles coated in gold and nickel, unfunctionalized particles were subjected to a magnet observed under a brightfield microscope. Forward motion was captured by placing Cerberus particles suspended in PBS on a clean glass slide and a magnet was placed near the particles. Rotational motion was also evaluated by placing a magnet near the droplet which was subsequently moved 90 degrees.

CHAPTER 3 MANUFACTURE OF FUNCTIONALIZED CERBERUS PARTICLES

3.1 Metal evaporation fabrication of Cerberus particles

3.1.1 Dispersive layer assembly

Particles were suspended in diH_2O followed by a 7 minute centrifugation at 2000xG. The supernatant was aspirated and the particles were resuspended in 50% ethanol followed by another centrifugation cycle. Again, the supernatant was aspirated and the particles were resuspended in 100% ethanol to a final concentration that would minimize clustering of particles when dried onto glass slides. For the 4 μm silica particles, this concentration was around $5.2x10^7$ particles/mL. For the 1 μm silica particles, this concentration was around $5.02x10^9$ particles/mL. Glass slides were sonicated in diH_2O for 30 minutes then dried under a nitrogen gas stream to clean prior to particles spotted onto the surface. Cleaned particles were spotted onto the cleaned glass slides using 2-3 μL droplets and dried at room temperature (Figure 3-1).

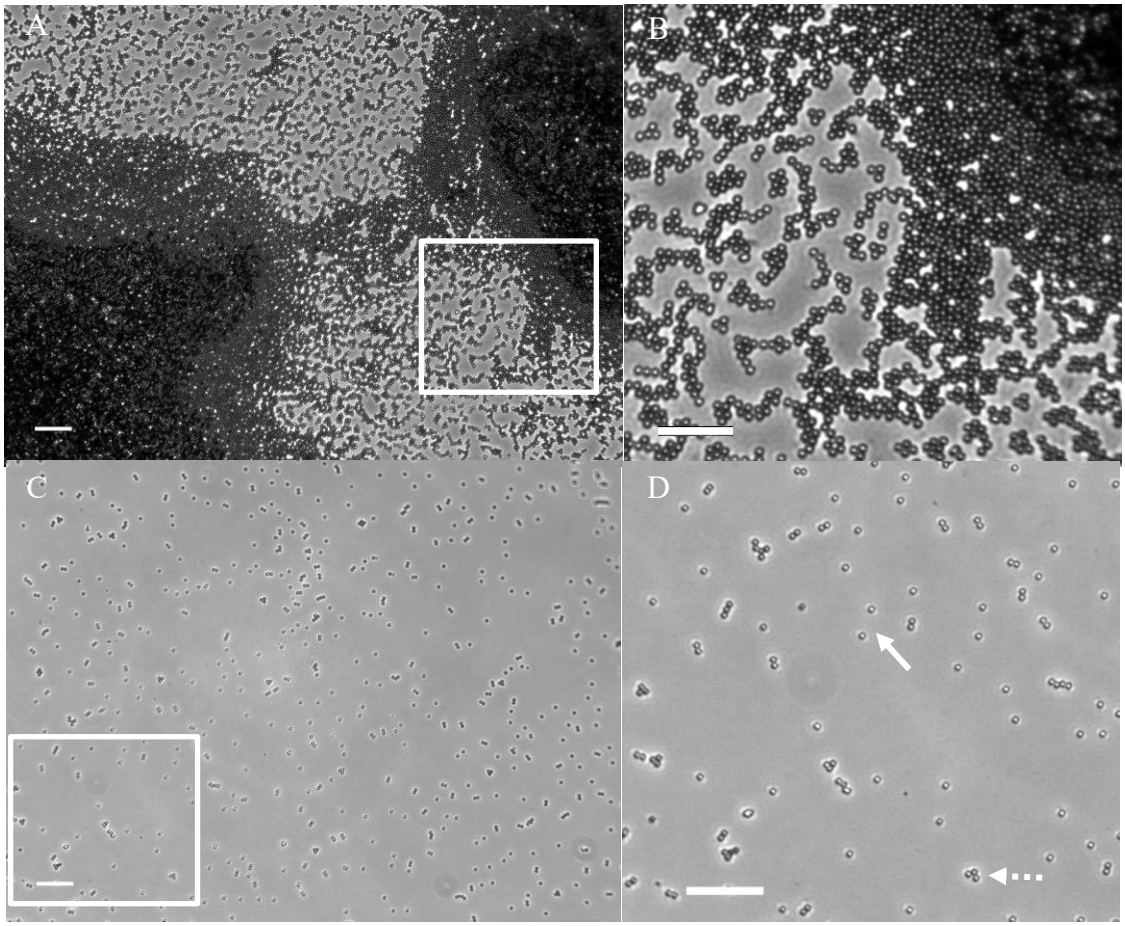

Figure 3-1. Brightfield images of 4 μm silica particles dried on glass. (A) Non-ideal concentration of particles showing clustering and stacking of particles and an ideal concentration. (B) Zoomed in view of white box in A (C) Ideal concentration where individual particles can be discriminated between and minimal clustering exists. (D) Zoomed in view of white box in C. A and C were taken at 10x magnification and all scale bars are 50 μm.

In order to quantify the dispersity of particles, the average number of neighbors was determined. For a completely disperse layer, each particle would have 0 neighbors while a monolayer would result in close packing and each particle would have 6 neighbors. Thus we define dispersity as the number of neighboring particles/particle. For each particle in the frame, the number of particles it was touching was counted. Only 1-5 frames for each concentration of particles was counted and was assumed to be a representative assessment. The quantification is shown in Figure 3-2. An example of the dispersive analysis in ImageJ is in Appendix A.

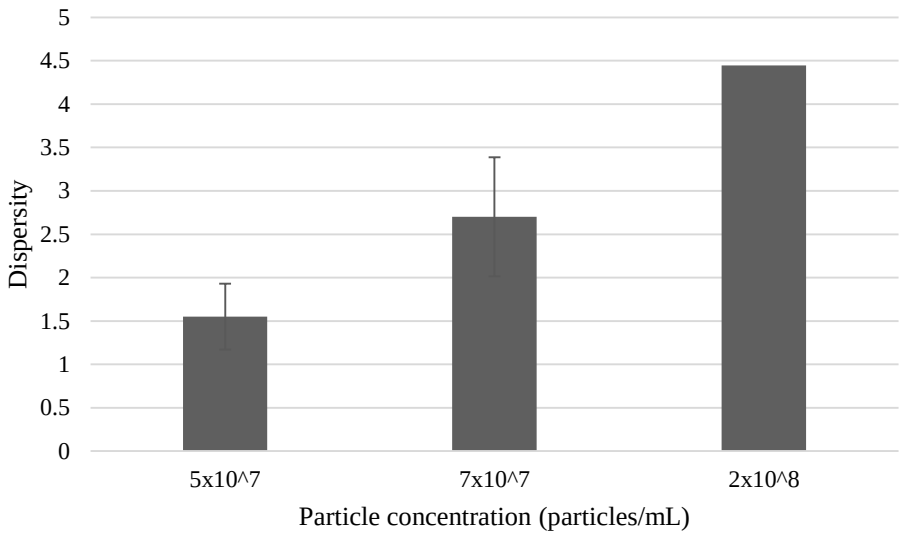

Figure 3-2. Dispersity of particles at different concentrations. As the concentration of the particles decreases, the dispersity also decreases. Dispersity was measured as the number of neighboring particles per particle in a frame. 0 is complete dispersity where no particles are touching, and 6 is no dispersity and close packing of particles occurs. Error bars are standard deviation across 5 frames of view counted except for 2x10^8 condition where only one frame was measured.

3.1.2 Metal evaporation glancing angle characterization and optimization

Glass slides containing a dispersive layer of silica particles were initially placed at a 45 degree angle in the metal evaporator on a slide holder made of glass slides. A specially designed slide holder was developed to increase angle specificity, repeatability, and yield of particles per metal evaporation process (Figure 3-3). Prior to the slotted design glass slide holder, a maximum of 16 glass slides resulting in the fabrication of ~1 million Cerberus particles was possible. With the new design, 13 glass slides per holder, with 2 holders (26 total glass slides) could be processed at one time resulting in ~3 million Cerberus particles fabricated per metal evaporation process.

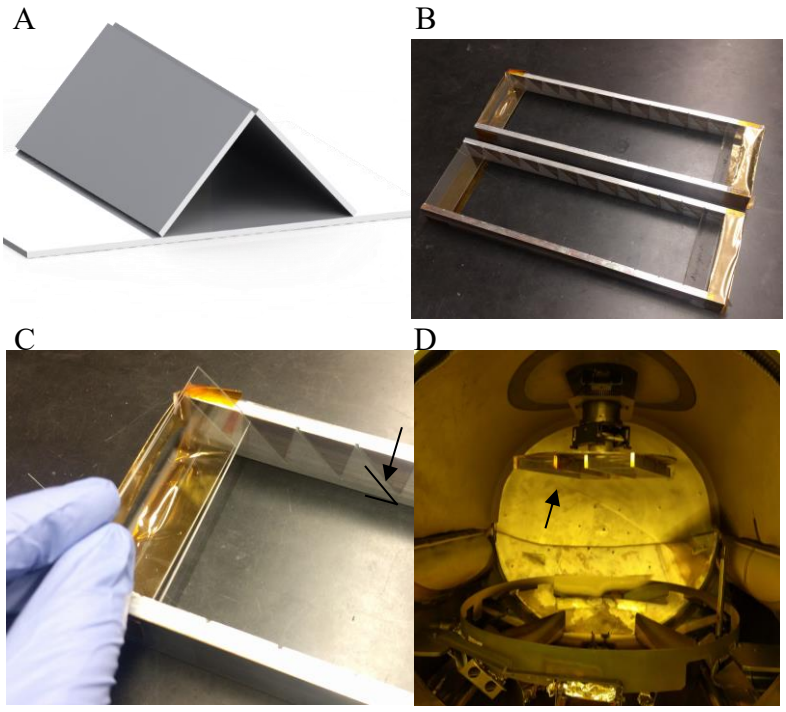

Figure 3-3. Glass slide holders control the angle of deposition. (A) First glass slide holder design which holds 2 slides. (B) 13 glass slide holder milled out of aluminium. The slots are at a 45 degree angle. (C) Insertion of a glass slide makes control of the angle consistent. (D) 2 aluminium slide holders in the metal evaporation chamber.

In order to evaluate metal evaporation as a process for making Cerberus particles the thickness of metal evaporation layer, thickness-to-diameter ratio of metal evaporation layer, angle of deposition, and the metals evaporated were assessed. Scanning electron microscopy (SEM) (Hitachi SU8230) was used to characterize the evaporation process.

Silica particles were subjected to metal evaporation of a single metal at one glancing angle to determine the effects of the angled deposition (Figure 3-4 A & B). Particles were not removed from the substrate post evaporation in order to show the orientation of the particles and the metal coating. SEM shows that with two different metals, Au and Ni, that the glancing angle deposition creates an angled layer. This is in opposition of particles that were subjected to non-glancing angle metal evaporation (Figure 3-4 C & D). Before

removal from the substrate, there is no 'line' between the silica particle and the metal layer. Upon removal from the substrate, the two sides of the particle can be seen, making a Janus particle (Figure 3-4 D). Next, the combination of two glancing angle depositions was tested. 100 nm Au was evaporated first at one glancing angle, the particles were rotated 90 degrees, and 100 nm Ni was evaporated at the second glancing angle (Figure 3-4 E). Particles before removal from the substrate shows a thick layer of metal, especially in the center at the "overlap" region of the two evaporated metals (Figure 3-4 E, *). After particle removal from the substrate, particles were redeposited onto a substrate for imaging (Figure 3-4 F). This reorients the particles to see the silica region with the two metals and ensures that the metal did not come off in the particle removal step. Particles were evaluated with SEM to confirm metal evaporation further (Figure 3-4 G). Particles that remain on the original substrate do not show any silica through the thick metal layer. After the particles are removed from the substrate and reimaged with SEM/EDS, the orientation of each particle changes and the shielded silica is revealed showing the Cerberus nature of the particle (Figure 3-4 H). Three distinct regions can be seen from the images.

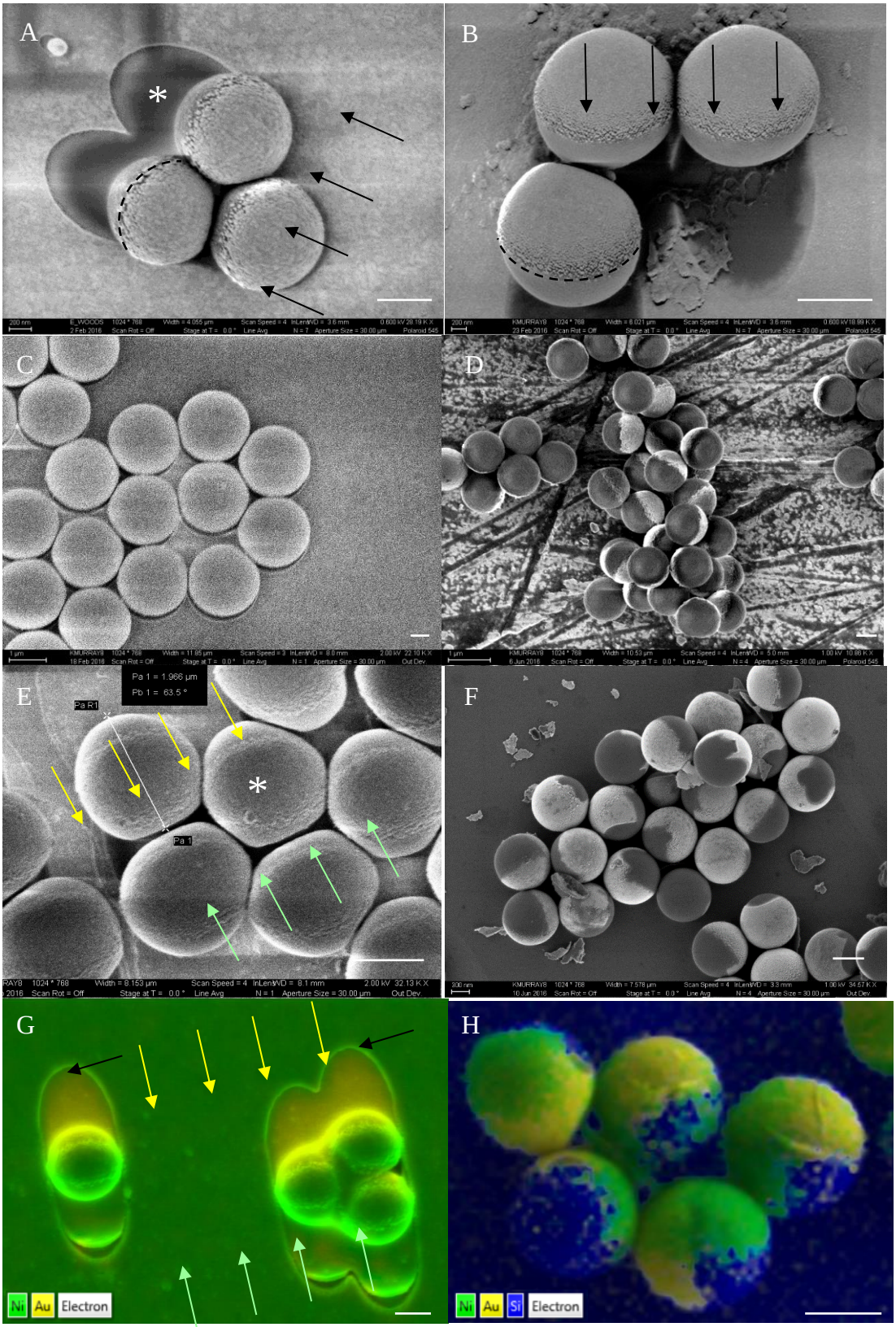

Figure 3-4. Glancing angle metal evaporation creates three chemically distinct regions. SEM image analysis of 1 µm silica particles after a 100 nm metal evaporation of

gold (A) and nickel (B) at a glancing angle prior to removal from the substrate. Angle of deposition is shown with black arrows. The glancing angle metal evaporation can be seen by the line between the silica and metal layer (dashed line). Additionally, a shadow region, *, is created on the substrate from the particle. The glancing angle coated particles can be compared to the non-glancing angle coated particles in (C) where there are no visible layer lines. (D) Particles without glancing angle post-removal reveals the two hemispheres of the Janus particle. (E) SEM of 1 μm particles with two glancing angle metal evaporations of 100 nm thickness before removal from substrate. There is a region of overlap of the two metal layers, indicated by an *. (F) Particles with two glancing angle metal evaporation processes post-removal reveals three regions and more than half of the particle is coated. (G) EDS analysis of gold (yellow) and nickel (green) metal evaporation at opposing glancing angles. Au was deposited first from the 'top' of the image and Ni was deposited second from the 'bottom' of the image as shown by the corresponding colored arrows as in E. The shadow of the particle shields the substrate from Ni deposition (black arrow), not covering the Au which was deposited first. Close packing of particles shown in the right cluster of 3 particles shields neighboring particles from full glancing angle deposition. (H) Particles removed from the glass substrate and redeposited onto a silica substrate reveals the three distinct regions: Au in yellow, Ni in light blue, and silica in purple. All scale bars are 0.5 μm.

3.1.3 Particle size to metal evaporation thickness analysis

It was important to characterize the particle size to metal evaporation thickness ratio for the development of a customizable and functional particle. Particle sizes of 4, 1, and 0.15 μm were tested with thicknesses of 100, 30, and 20 nm per metal evaporation layer. A 100 nm thickness metal evaporation layers created a thick coating across all particle diameters tested. For a 1 μm particle, 100 nm is 1/10 the diameter of the particle, greatly increasing the size of the particle form 1 μm to 1.2 μm in the overlap region and results in clusters of particles stuck together in the metal layers (Figure 3-5 A). It is important for the particles to be single particles rather than a clump of multiple particles as these particles are intended to be functionalized. At metal evaporation thickness layers at 20 and 30 nm reduce the thickness-to-size ratio to 1/50 and 1/30, respectively, for 1 μm particles (Figure 3-5 B). 4 μm particles were also examined with 20 and 30 nm for a thickness-to-diameter ratio of 1/50 and ~1/133 (Figure 3-5 B & C). There was little to no clumping from any of

these combinations of particle size to metal thickness at 20 or 30 nm layers. From this point further, metal evaporation layers were performed at a thickness of 20 or 30 nm. Additionally, 150 nm silica particles were processed with glancing angle metal evaporation layer thicknesses of 20 nm, resulting in a thickness-to-diameter ratio of 2/15 (Figure 3-5 D). This ratio is almost equivalent to the 100 nm thick layers on a 1 μm particle. Additionally, it can be seen that surface roughness has increased for the smaller particles. Overall, the thickness of these multilayer depositions should be scaled to diameter of the particle, and for 1 and 4 μm particles, the thickness should be in the range of 20-50 nm.

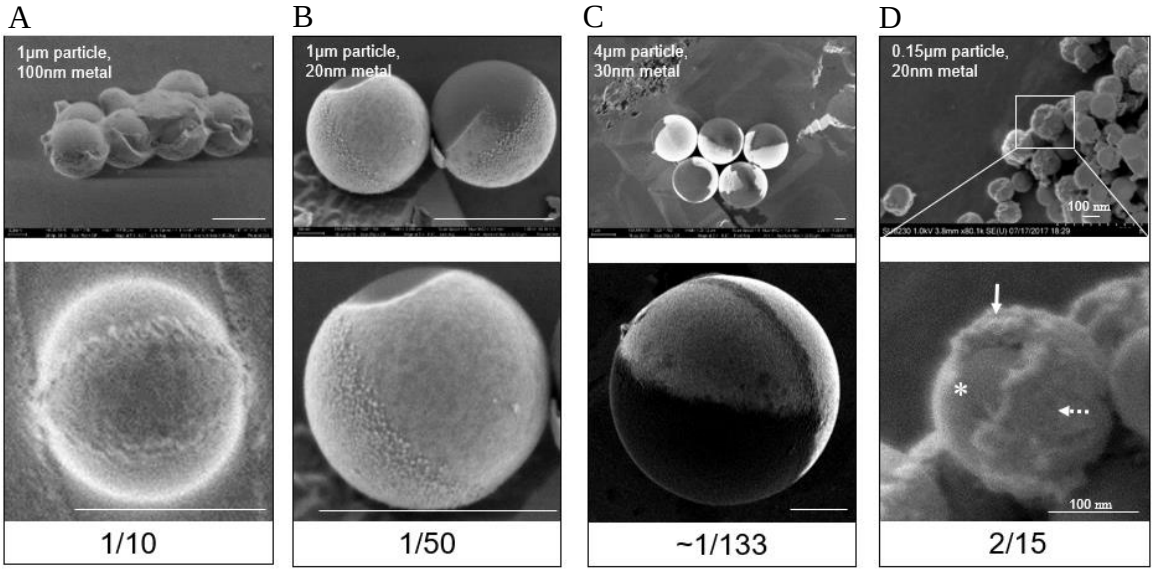

Figure 3-5. Metal evaporation thickness to particle diameter is optimal between 1/50 – 1/150 (A) 1 μm particles with 100 nm metal evaporation layers of Au and Ni at two glancing angles post removal from original substrate. Zoomed in single particle, prior to removal from substrate. (B) 1 μm particle with 20 nm Au and Ni layers. (C) 4um particles with 30 nm Au and Ni layers. (D) 150 nm silica particles with 20 nm gold and 20 nm nickel metal evaporation layers at two distinct angles. Zoomed in view of a single particle. Solid arrow indicates the nickel layer, dashed arrow indicates gold layer, and * indicates silica particle. All scale bars are 1 μm unless otherwise noted.

3.1.4 Variation in glancing angle metal evaporation

The angle of deposition was also evaluated by using a variable glass slide holder which the angle could be manipulated prior to each subsequent deposition. As shown in

Figure 3-6, the particles were subjected to metal evaporation of Au at a 60 degree angle, then rotated to a 30 degree angle for a Ni layer deposition. While the rotation angle is 90 degrees as the previous methods above, the steeper angle resulted in more shielding between particles.

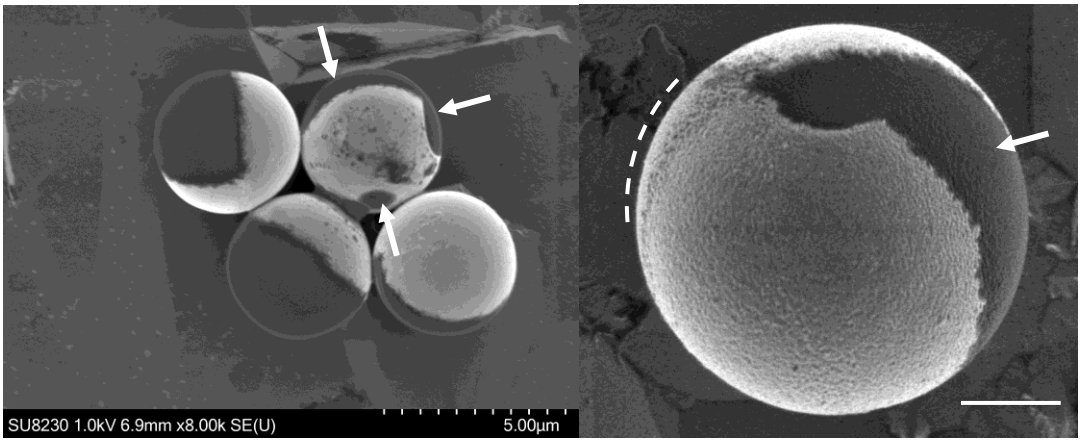

Figure 3-6. Difference in angle between glancing angle metal evaporation determines region of particle coated. (A) A representative image of 4 µm particles evaporated at 60 degrees followed by 30 degrees (90 degree rotation). There was more shielding observed as less than ¾ of the particle is coated compared to the particles evaporated at 45 and 45 degrees, arrows. (B) 4 µm particle with glancing angle deposition of Au at 60 degrees followed by glancing angle metal evaporation of Ni at 60 degrees (rotated 120 degrees). Only a small region, dashed line, is overlapped with both evaporated metal and a small region is uncoated, arrow. Scale bar = 1 µm.

After we determined that we could evaporate two metals at combinations of 30, 45, and 60 degrees, we attempted metal evaporation of more than 2 metals. In Figure 3-7 A, three metals (Au, Ni, Cu) were evaporated onto 4 µm particles at different glancing angles, thus creating 4 regions on a single particle. The EDS analysis shows separation of the metals although there is a large region of overlap for each subsequent layer. Au was evaporated first with the particles at 60 degrees. The particles were rotated to 0 degrees and Ni was evaporated. Finally, the particles were rotated another 60 degrees to the opposite side and Cu was evaporated. With the total range of the rotation of the particle

being 60 degrees, there should be 120 degrees without metal. This can be seen by the purple, uncoated silica from the EDS analysis, dashed line.

Additionally, four metals, Au, Ni, Cu, and Al, were deposited onto 4 μm particles at 60, 30, 0, and 30 degrees of 30 nm thicknesses each. EDS shows the successful deposition of each of these metals. The Au and Ni are mainly on the face of the particle facing upwards while the Cu and Al are mainly on the face of the particle facing downwards but are still visible.

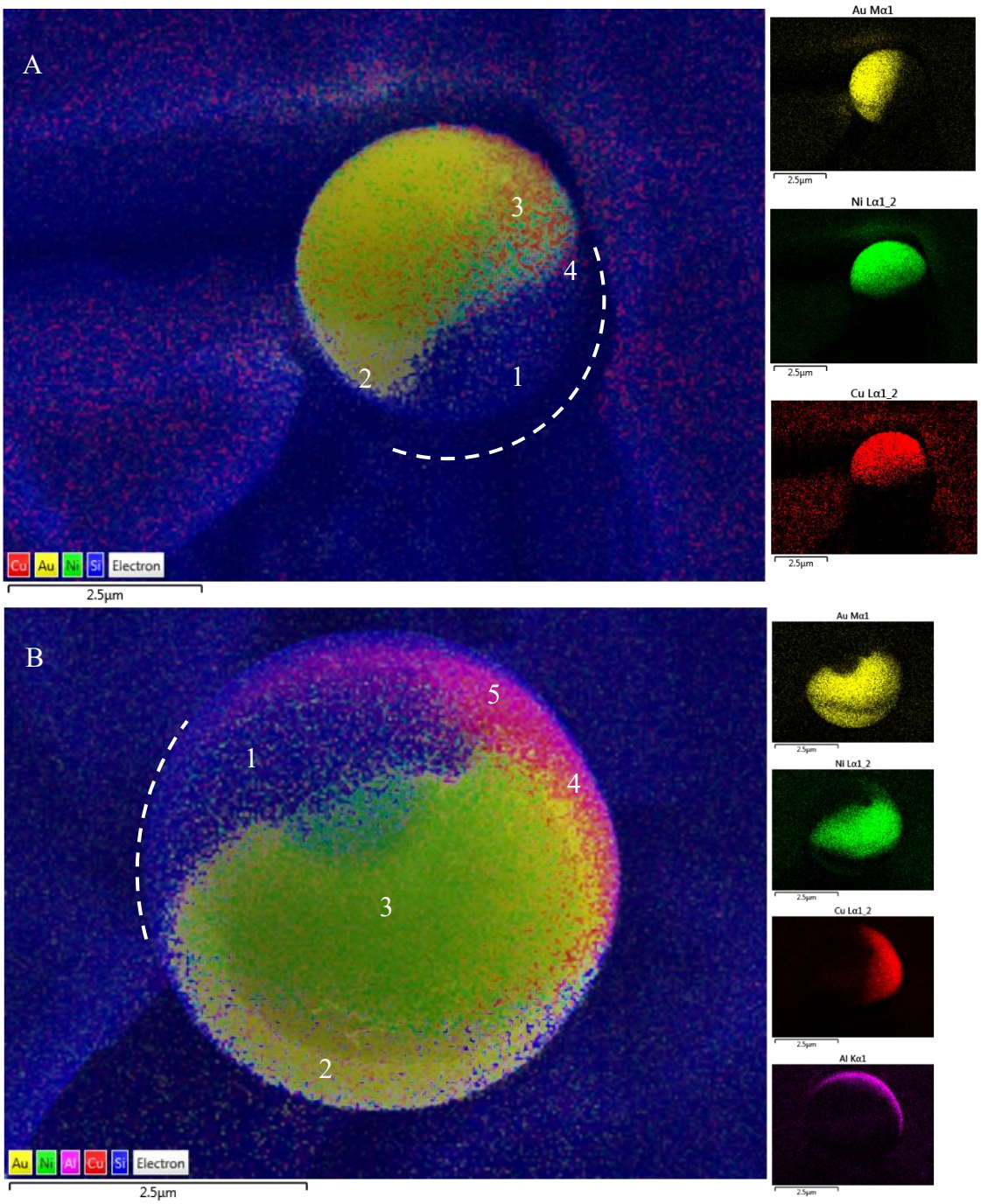

Figure 3-7. Glancing angle metal evaporation can increase number of regions. (A) 4 µm silica particle with glancing angle deposition of Au, Ni, and Cu at 30, 0, and 30 degrees of 30 nm thicknesses each. Dark blue, 1, is silicon, Yellow, 2, is gold, Green, 3, is nickel, and Red, 4, is copper. Dashed line indicated region of uncoated silica particle. (B) 4 µm particle with glancing angle deposition of Au, Ni, Cu, and Al at 60, 30, 0, and 30 degrees of 30 nm thicknesses each. Dark blue, 1, is silicon; Yellow, 2, is gold; Green, 3, is nickel; Red, 4, is copper; Purple, 5, is aluminum. Dashed line indicated region of uncoated silica particle. Scale bars on bottom left are 2.5 µm.

3.2 Optimization of the functionalization of Cerberus particles

After metal evaporation optimization and the creation of the three regions (silica, gold, nickel), the particles are functionalized. The functionalization protocol was optimized in order to achieve signal above background and achieve spatial segregation. While flow cytometry allowed for assessment of the presence of the three proteins, this does not allow for analysis of region specificity of the conjugation that we expect to achieve. Thus, both methods are used to assess the functionalization. The spatial segregation of the proteins conjugated onto the surface of the Cerberus particle was then assessed via fluorescent microscopy. After functionalization, particles were spotted onto glass with ProLong Diamond and a cover glass, let dry overnight, and imaged with a PerkinElmer spinning disk fluorescent microscope.

Initially, two functionalization protocols were tested. In the first protocol, gold was functionalized first with biotin-PEG-thiol (Figure 3-8 A). The silica region was then activated with APTES and conjugated BSA. Then SA is added to bind to the biotin, finishing the gold region functionalization. Lastly, HIS-GFP is conjugated. Antibody staining was performed with BSA stained with 405, and SA was prelabeled with APC. In the second protocol, biotin-PEG-thiol was conjugated to the gold region followed directly by SA which binds to the biotin (Figure 3-8 B). Then the silica region was activated with APTES and BSA was conjugated to the activated silica. Finally, HIS-GFP was conjugated to the particles. Flow cytometry results of the two protocols compared to negative control particles are shown in Figure 3-9. Protocol 1 (A) had positive signal in the DAPI and APC channels indicating the presence of BSA and SA on the particles. Protocol 2 (B) had positive signal in the DAPI channel indicating the presence of BSA on the particles. Both

protocols had no increased signal in the FITC channel indicating no presence of GFP. While this indicates the presence of no protein, the protocol was modified for antibody staining of the GFP to increase the signal of the protein for flow cytometry.

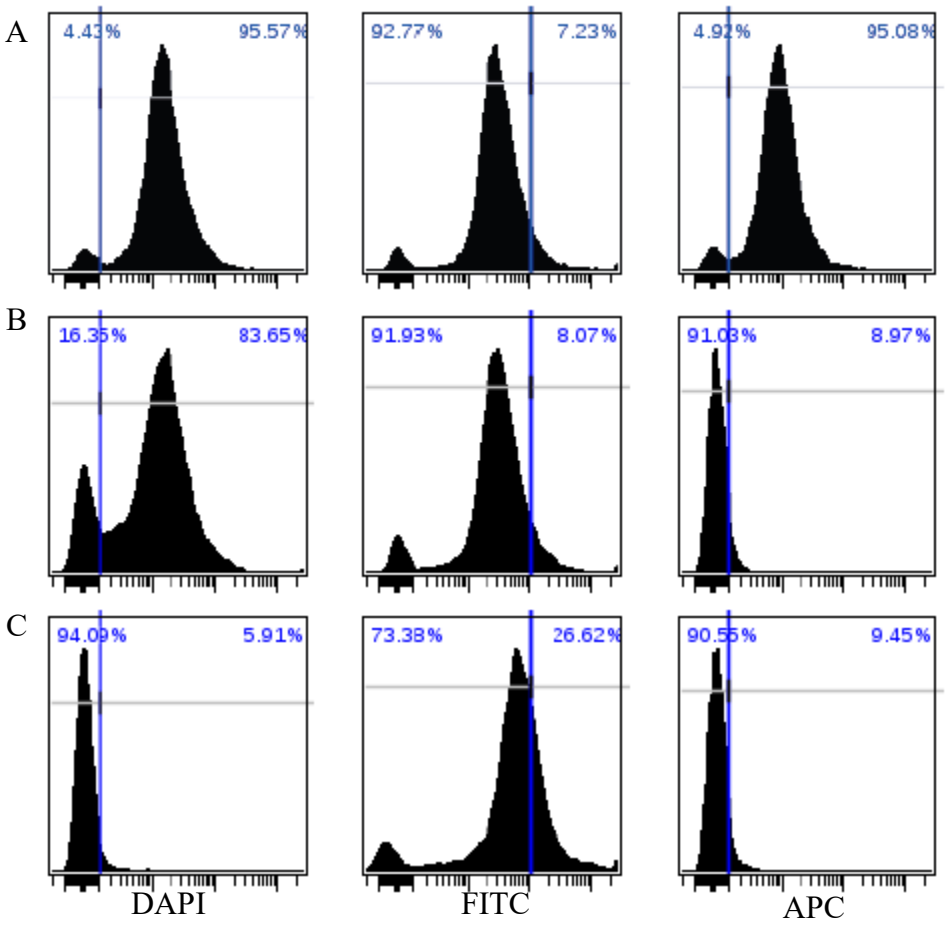

Figure 3-8. Flow cytometry analysis of two functionalization protocols do not have HIS-GFP binding to particles. (A) Biotin-PEG-thiol is added first, followed by APTES/BSA. Then SA is added to bind to the biotin and lastly HIS-GFP is conjugated. BSA is stained in 405, DAPI channel; GFP is stained in 488, FITC channel; and SA is prelabeled with APC. (B) A second conjugation order was tested. First, Biotin-PEG-thiol was conjugated followed by SA. Then APTES/BSA was conjugated. Finally, HIS-GFP was allowed to bind to the particles. Antibody staining was performed. (C) Negative control particles with no protein conjugation.

3.2.1 HIS-GFP concentration optimized for functionalization of Cerberus particles

The results from Figure 3-8 show that there was no HIS-GFP protein conjugated to the particles. A test was performed to optimize the concentration of HIS-GFP to bind the

Cerberus particles. Cerberus particles were incubated with only HIS-GFP at varying concentrations from 0 to 50 ng/mL for 1 hour. After incubation and washing to remove excess protein, flow cytometry was performed (Figure 3-9). Gates were based on the negative control. It was determined that 6.25 ng/mL HIS-GFP was the optimal concentration based on the regression.

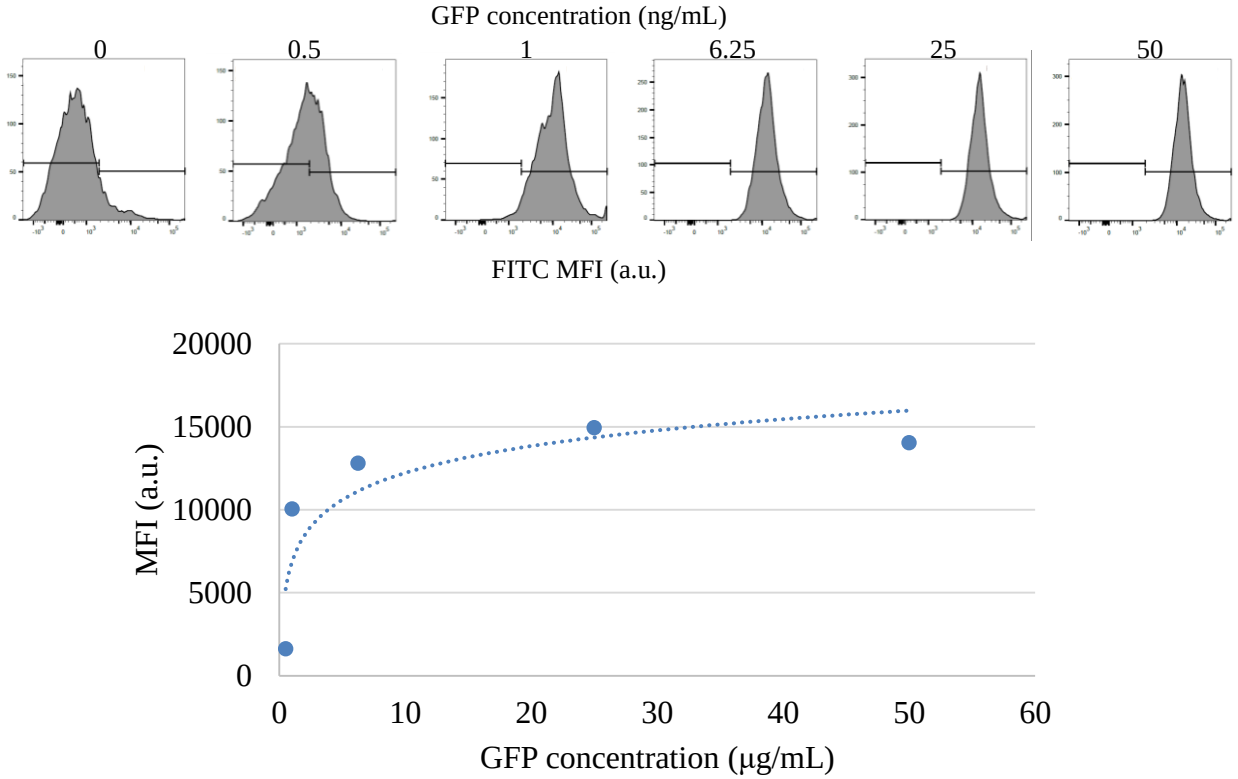

Figure 3-9. HIS-GFP concentration optimization for Cerberus nickel functionalization. (A) Flow cytometry histograms display the shifting peak for the protein conjugated to the particles. (B) Plot of the mean fluorescent intensity (MFI) for each of the concentrations used.

3.2.2 Cerberus particle functionalization optimization to achieve spatial segregation

Additional functionalization protocols were examined in order to attempt increased spatial segregation. Alteration of the order of protein functionalization did not improve the spatial segregation as shown in Figure 3-10. In protocol 1, gold is activated with thiol-PEG-biotin, followed by silica activation with APTES and subsequent functionalization

with IgG. IgG was used instead of BSA in this conjugation step as the BSA was passively adsorbing as a blocking agent to the entirety of the particle (images not shown). Next, SA is added, binding to the biotin on the gold. Finally, HIS-GFP is functionalized to the nickel using the optimized concentration. Antibody staining is then performed with IgG stained with 405, GFP stained in 488, and SA was prelabeled with APC. Protocol 2 first activates the silica with APTES and subsequent functionalization with IgG. Then thiol-PEG-biotin is added to bind the gold region. SA is functionalized to the biotin followed by the HIS-GFP to the nickel. Antibody staining was then performed as stated in Protocol 1.

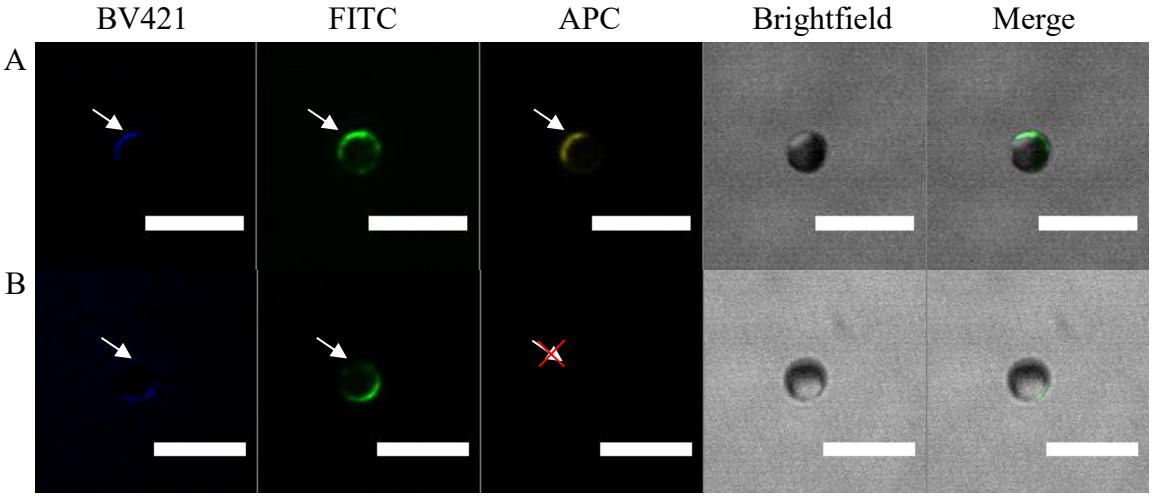

Figure 3-10. Fluorescent images of Cerberus particle spatial segregation optimization which have undergone two functionalization protocols. (A) Functionalization of the gold region first with thiol-PEG-biotin, then the silica side with APTES/IgG. SA and HIS-GFP are added last. (B) Functionalization of the silica side with APTES/IgG, followed by the gold side with thiol-PEG-biotin and SA and the HIS-GFP functionalization last. Scale bars are 10 μm.

From the results in Figure 3-10, it was clear that of the two protocols, it was best to functionalize the thiol-PEG-biotin to the gold region first, then perform the silica activation and functionalization with APTES/IgG before binding SA. The APTES activation is a strong chemical process which could have denatured the protein or dissociated the APC fluorophore which was prelabeled on the protein. This protocol was then tested on Cerberus particles which had been fabricated with 30 nm gold followed by 30 nm nickel. There had

been evidence of some specific binding however there was additional overlap where the metal overlapped. We theorized that a thicker metal layer would cover the underlying chemical region to prevent unwanted conjugations. Specifically, we wanted a thicker gold region to prevent silica activation from occurring underneath the metal layer, and we wanted a thicker nickel region to prevent gold-thiol or silica activation underneath the metal layer.

Flow cytometry results of 1 μm silica Cerberus particles with 30 nm metal layer thicknesses of gold/nickel are shown in Figure 3-11. Particles were assessed in the BV421, FITC, and APC channel corresponding with the fluorescent labels of the conjugated proteins, IgG, GFP, and SA, respectively. There is a distinct population of positive signal compared to the negative control (not shown). Quantification of flow cytometry MFI shows a higher signal in the individual controls and the trifunctional particles compared to the negative control particles. Additionally, of all the trifunctional particles, 75% of them are gated positive for all three channels, indicating they are conjugated with all three proteins, thus are trifunctional. This can also be seen in the 3D graph, where particles in red/orange/green are triple positive (Figure 3-11 D).

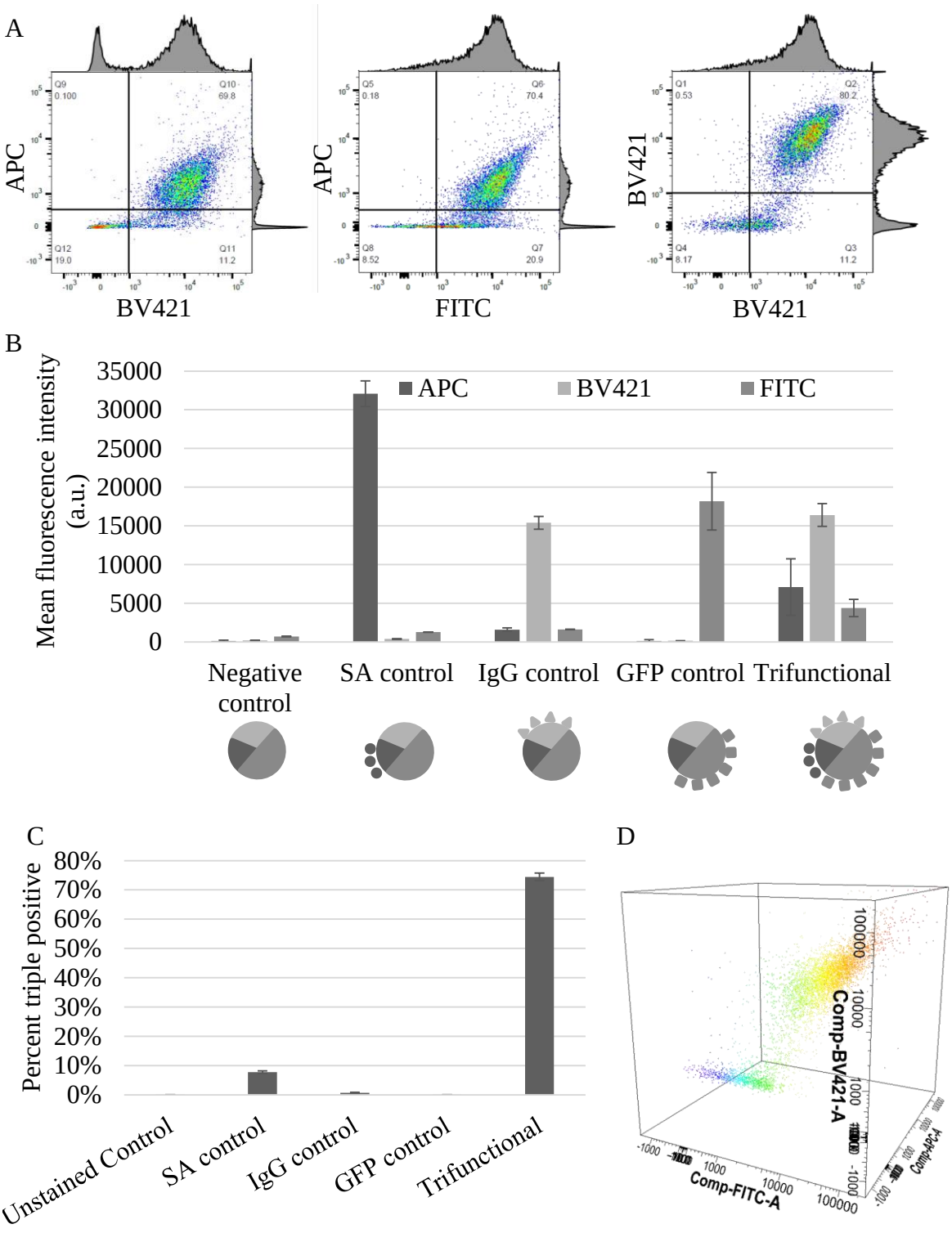

Figure 3-11. Flow cytometry analysis of trifunctionalized Cerberus particles with optimized protocol. (A) Fluorescent intensity plots with corresponding histograms of trifunctionalized particles. Plot from left to right: APC vs. BV421, APC vs FITC, BV421 vs. FITC. Gating is shown for positive signal in each channel. (B) Quantification of fluorescent signal from flow cytometry. Experiment was performed in triplicate, with at

least 10,000 particles assessed per sample. Error bars indicate standard deviation. (C) Functionalization efficiency in terms of percent of particles expressing positive signal for the BV421, FITC, and APC channels. (D) 3D rendering of flow cytometry data with two populations visible, the majority being in the upper right-hand corner being positive for BV421, FITC, and APC.

From the fluorescent images, each of the three proteins segregate to various regions on the particle (Figure 3-12 B & C). On the brightfield view, the lightest part is the non-coated silica base particle. The dark region is the metal, gold and nickel. While the distinction between the gold and nickel regions are not clear on from the brightfield, there is evidence on the fluorescent images of these distinct regions. The SA protein is labeled in APC (yellow) and is targeted to the gold region of the Cerberus particle. The IgG protein is labelled in 405 (blue) and is targeted to the silica region of the Cerberus particle. The HIS-tagged GFP protein is labeled in 488 (green) and is targeted to the nickel region of the Cerberus particle.

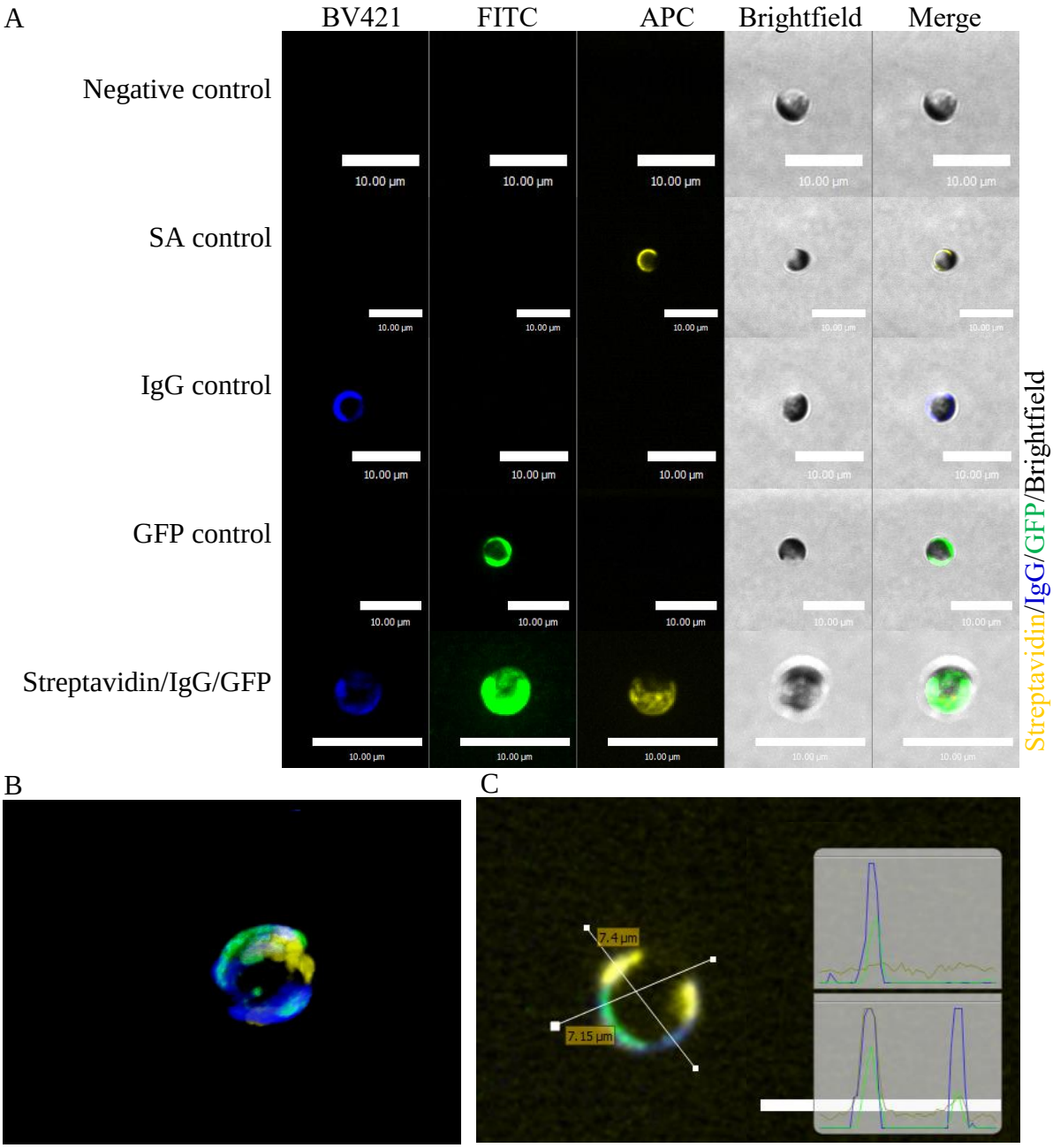

Figure 3-12. Fluorescent imaging of trifunctionalized Cerberus particles with optimized protocol resulting in spatial segregation of protein against control particles. (A) Single protein controls and trifunctional particles with SA labeled in APC (yellow), IgG labeled with AlexaFluor 405 (blue), and GFP labeled in FITC (green). Spatial segregation can be observed. Scale bars are 10 µm. (B) 3D rendering of a single particles. (C) 2D view of single particle with spatial segregation of fluorescent signal and intensity line profile. All scale bars are 10 µm.

The specificity of the conjugations to each chemically distinct region was evaluated by performing the optimized protocol on Janus particles that were coated in either gold or

nickel. The particles were functionalized as above and imaged via confocal microscopy. Representative images are in Appendix A-2 for gold Janus particles and Appendix A-3 for nickel Janus particles. Thiol-PEG-biotin and APTES conjugation methods appear specific to gold and silica, respectively. There is some overlap region of the conjugation as indicated by white regions of the 3D image. Analysis of the nickel Janus particles shows HIS-GFP binds to both nickel and silica regions of the particles. While we expected HIS-GFP to only bind nickel, there was non-specific binding of the HIS-GFP to the silica.

The optimization of the functionalization of Cerberus particles is summarized in the table below (Table 3-1). The two optimizations assessed were the order of functionalization and the thickness of metal evaporation layers.

	Protein functionalization order	Metal evaporation thickness	Trifunctionalization	Spatial segregation
Fig 3-7	Thiol-PEG-biotin APTES/BSA SA HIS-GFP	1 μm particle 20 nm Au 20 nm Ni	No	Not tested
Fig 3-7	Thiol-PEG-biotin SA APTES/BSA HIS-GFP	1 μm particle 20 nm Au 20 nm Ni	No	Not tested
Fig 3-9	Thiol-PEG-biotin APTES/IgG SA HIS-GFP	4 μm particle 20 nm Au 20 nm Ni	Yes	No
Fig 3-9	APTES/IgG Thiol-PEG-biotin SA HIS-GFP	4 μm particle 20 nm Au 20 nm Ni	No	No
Fig 3-10	Thiol-PEG-biotin APTES/IgG SA HIS-GFP	4 μm particle 30 nm Au 30 nm Ni	Yes	Yes

Table 3-1. Summary of functionalization protocol for gold/nickel/silica Cerberus particles.

3.3 **Functionalized Cerberus particle applications**

3.3.1 Magnetic potential for nickel Cerberus particles

Nickel is a well-known magnetic metal[6,30]. These magnetic properties can be used for many application including magnetic separation[31] and remote control cell activation by particles[32]. Two magnetic motions were briefly explored here as a preliminary test for Cerberus particles which contain both silica and gold in addition to the nickel. Forward motion was captured by placing a droplet of Cerberus particles on a clean glass slide and a magnet was placed near the droplet (Figure 3-13). Particles moved towards the magnet and collected at the edge of the water droplet.

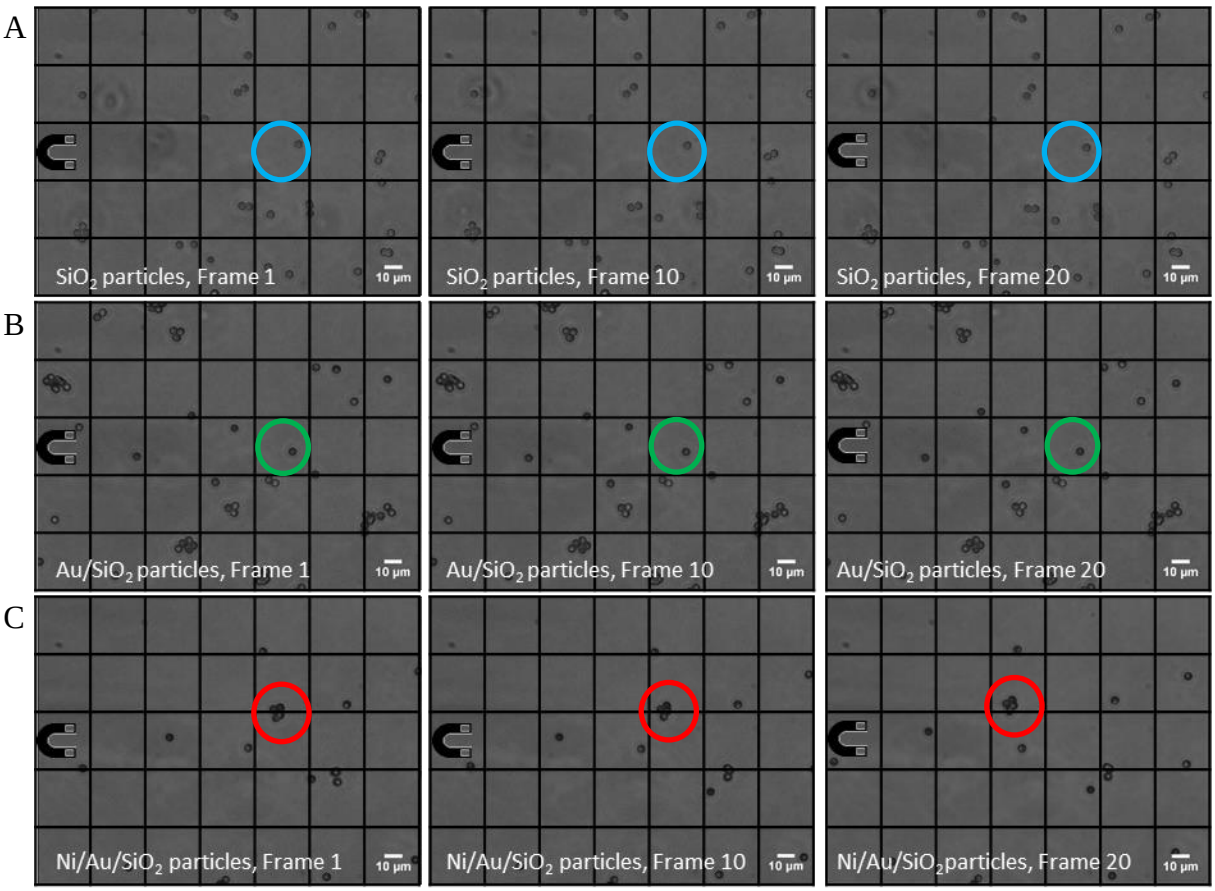

Figure 3-13. Nickel Cerberus particles exhibit forward motion when a magnet is applied. (A) 4 µm silica particles prior to metal evaporation process, that when a magnet is applied, do not move forward. Blue circle outlines a single particle. Frames 1, 10, and 20 are displayed. (B) 4 µm Au/silica Janus particles do not move forward towards an applied magnet. Green circle outlines a single particle. Frames 1, 10, and 20 are displayed. (C) 4 µm Ni/Au/silica Cerberus particles exhibit forward motion when a magnet is applied. A distinguishable group of particles are outlined in red as they move across the frame from (2,5) to (2,4) over frames 1, 10, and 20 (displayed). Magnetic rotation of the same nickel Cerberus particles, where blue circles are initial orientation and red circles are final orientation after rotation. Scale bars are 10 µm.

Rotational motion was also tested (Figure 3-14). A magnet was placed near the droplet then moved 90 degrees. Particles rotated according to the location of the magnet.

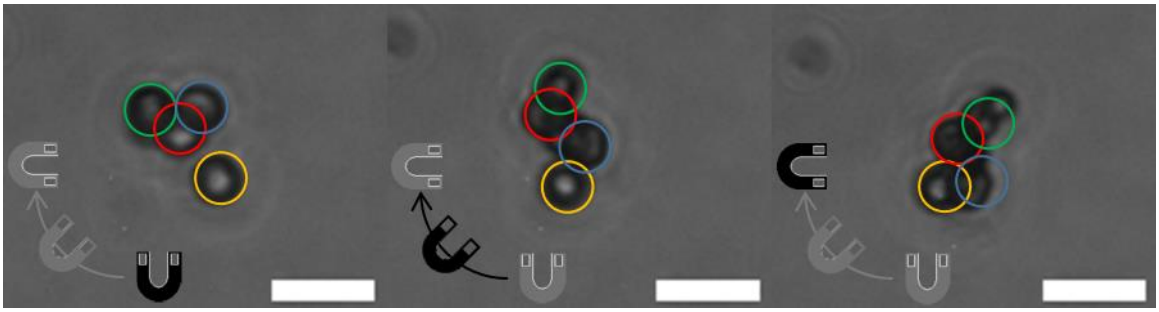

Figure 3-14. Nickel Cerberus particles exhibit rotational motion when a magnetic is applied. As the magnet is rotated from the bottom of the image to the left-hand side of the image, the particles rotate to face the magnet. Individual particles are outlined in different colors for ease of viewing. Scale bars are 10 μm.

Overall, these brief explorations of non-biologically functionalized Cerberus applications display the wide variety of potential applications for customizable, multifunctional particles.

CHAPTER 4 DISCUSSION OF ADVANTAGES AND CHALLENGES OF REPEATED GLANCING ANGLE DEPOSITION AND FUNCTIONALIZATION OF CERBERUS PARTICLES

We have shown that we can use repeated glancing angle metal deposition to create multi-region particles of various sizes and can functionalize a three-region Cerberus particle to produce spatial segregation. In optimization of the functionalization protocol, the order of protein conjugation and the influence of the thickness of metal evaporation layer was investigated.

In the fabrication of the multi-region particles, e-beam metal evaporation provided both advantages and challenges. E-beam metal evaporation occurs at a high vacuum, thus increasing the mean free path. By increasing the mean free path, the evaporating metal molecules travel in a straight line towards the substrate. This process provides very little coating to the sides of any features that are perpendicular to the surface of the substrate and coats only the surface facing towards the metal crucible source. Thus in the evaporation process, the particles are coated in the first metal on one hemisphere, making a Janus particle (Figure 2-1 A). Then the particles are rotated, and again the second metal coats one hemisphere of each particle. In fabrication of the Au and Ni Cerberus particles, the metal evaporation steps are performed 90 degrees from each other resulting in the final Cerberus particles being ¼ original base particle material (silica), ¼ first metal (gold) and ½ second metal (nickel). While these three regions are not the same size, having a second method to asymmetry can be beneficial for different applications.

In the process of rotating the particles and applying additional metal evaporation layers, there are regions of overlap between the layers. The difference in angle of deposition determines how much overlap there is. We believe the metals simply overlap and do not alloy. In SEM imaging of 1 μm particles with 100 nm metal evaporation layers, the overlap region appears thicker than the single metal regions. Additionally in EDS, the individual elemental mapping shows a lack of the metal underneath (Figure 4-1). Alloying would result in a more uniform signal and EDS coloring. Altering the thickness of the metal layers can change the EDS analysis of the metals as the voltage and current can be changed to better assess the surface or the internal material. The voltage used in the SEM analyses in this thesis was 1 kV and 10 μA at 3 mm working distance. EDS settings were 10kV and 10 μA at 10-15 mm working distance. XPS analysis could confirm this further and assess oxidation of the metals. There has been evidence of the diffusion between multilayer metal evaporation and growth of oxide layers, however this phenomenon is a slow process and should be investigated on a metal-to-metal basis[33]. Multilayer metal evaporation is a commonly used fabrication technique in nanofabrication and nanotechnology[34,35].

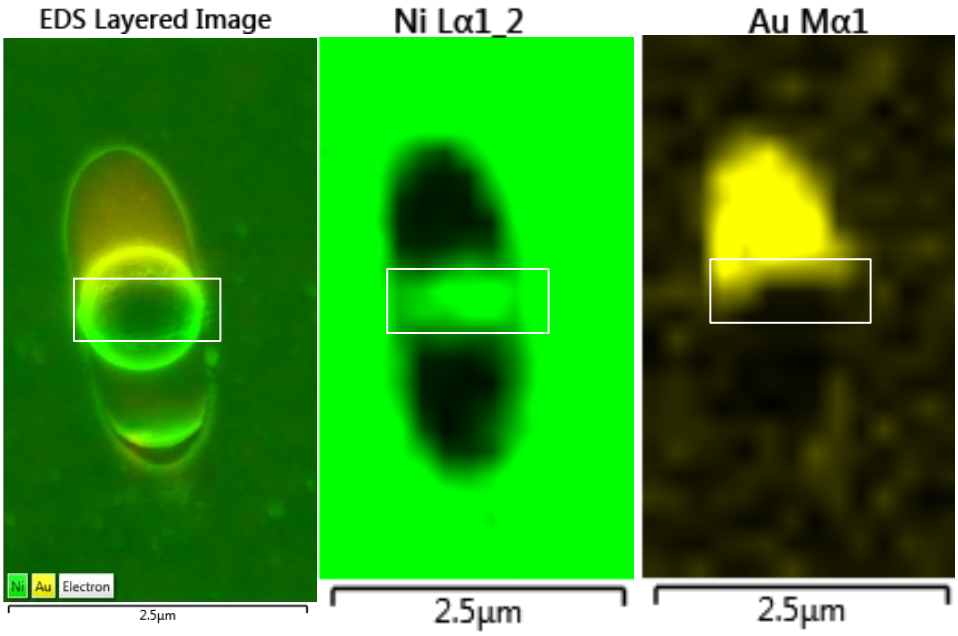

Figure 4-1. EDS imaging of a single particle with gold and nickel evaporated onto the surface. The region of metal evaporation overlap is highlighted by the white box. There is little gold signal compared to the gold regions and compared to the nickel overlap region.

We also examined how the angle of deposition can be changed, thus altering the geometry of the regions on the Cerberus particle. Unless otherwise specified, the glass slides holding the dispersive layer of particles were placed at 45 degrees for the first deposition and 45 degrees of the opposite direction for the second deposition. These angles can be increased, decreased, or added to as explored in Figure 3-5 and 3-6 to create different sized regions. For instance, a Cerberus particle could be made with the first deposition at 60 degrees and the second deposition at 45 degrees the opposite direction (105 degree rotation), thus creating at particle with 5/24 base particle (silica), 7/24 first metal, and 1/2 second metal. Additionally, a 4-sided particle could be made with 3 metal depositions occurring at 45 degrees, 0 degrees, and 45 degrees on the opposite direction, resulting in a 1/8 first metal, 1/8 second metal, ½ third metal, and ¼ unmodified particle.

During the optimization of the metal evaporation process, it became evident that in addition to the angle of deposition, the dispersity of the particles was also important for the

consistent coverage of both metals. A steeper angle produces more shielding from one particle to another, while a shallower angle has less of a shielding effect (Figure 4-2). This is also shown when producing Janus particles with no angle and monolayer packing is the most efficient[27]. The method for creating a dispersive monolayer involved sonicating the glass slides in diH_2O and washing the silica particles in ethanol. The difference in hydrophobicity causes the particle/ethanol mixture to spread out rapidly and dry with minimal clustering. Pretreating the silica particles with water compared to ethanol was also tested and there was no difference between the two methods in terms of functionalization ability. Dispersity was measured by counting the number of particles that touched each particle in one frame of view. An alternative dispersity measurement is the distance to the nearest neighboring particle for each particle. This method could increase multi-region particle fabrication consistency and the concentration of particles can be optimized for each angle of deposition to eliminate shielding from occurring.

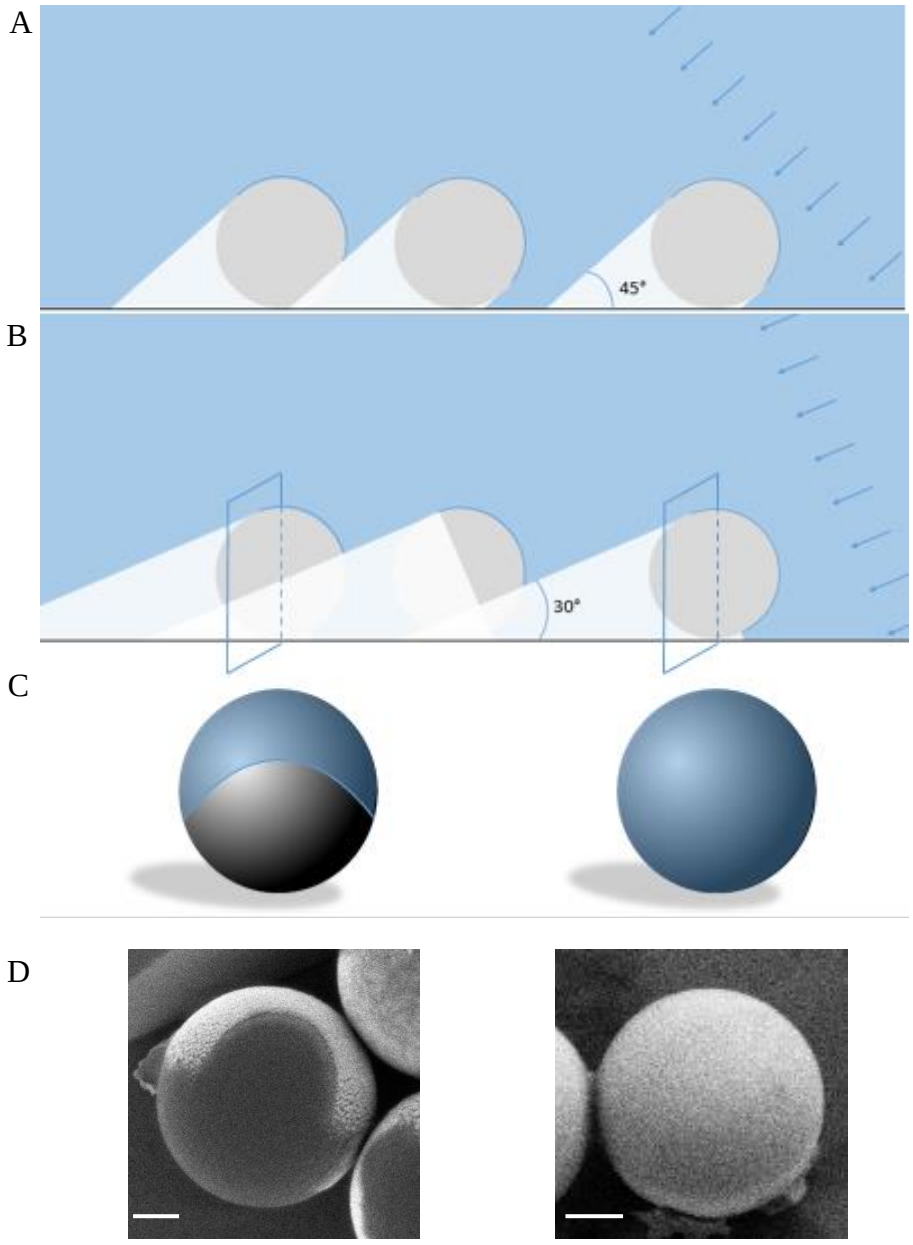

Figure 4-2. Glancing angle metal evaporation creates shadowing effect on neighboring particles. (A) A 45 degree glancing angle produces moderate shadowing on nearby particles. (B) A steeper 60 degree glancing angle (30 degree from horizontal) produces more shadowing effects as the rightmost particle can now shield the middle particles, compared to A. (C) Shadowing effects on particles can greatly alter the region of particle which is coated in the metal evaporation layer. The right particle has no shadowing and thus 50% of the particle surface (100% of the hemisphere) is coated in metal (blue), compared to the left particle which is subjected to shadowing resulting in only 25% of the particle surface (50% of the hemisphere) being coated in metal (blue). (D) SEM of particles demonstrating the shadowing effect. Scale bars are 200 nm (left) and 1 μm (right).

Additionally, the overall process of using metal evaporation has limitations in the types of particles which can be made. The evaporation chamber is heated due to the e-beam hitting the metal crucible in order to cause evaporation. In this study, we used silica particles which has a melting temperature of 1710°C. Other studies have used polystyrene particles, which have a melting temperature of ~240°C, to create Janus particles with metal evaporation[27]. There was no melting of the polystyrene particles however other polymeric particles can have melting temperatures between 70-200°C which may limit the extent of the use of this fabrication method.

It is important for each particle to be the same and have consistent fabrication of the multi-region particles. In thinking towards future applications of therapeutic delivery, the amount of drug, for instance, which needs to be delivered much be consistent. In this thesis we did not quantify the batch variability in fabrication due to the complication of working with particles. For verifying the multiple regions from repeated glancing angle metal evaporation, the particles were removed from the original substrate and redeposited onto a new substrate, allowing the particles to re-orient (Figure 4-3). This allows for the base particle to be visualized. Unfortunately the orientation is not controllable which makes verification of the fabrication difficult. Ideally, the particle regions could be measured across each particle batch to ensure consistent metal evaporation. This would involve measuring the angle between evaporation layers (Figure 4-3, red boxes) or area of particle covered, which has its own inherent problems in measuring a curved surface.

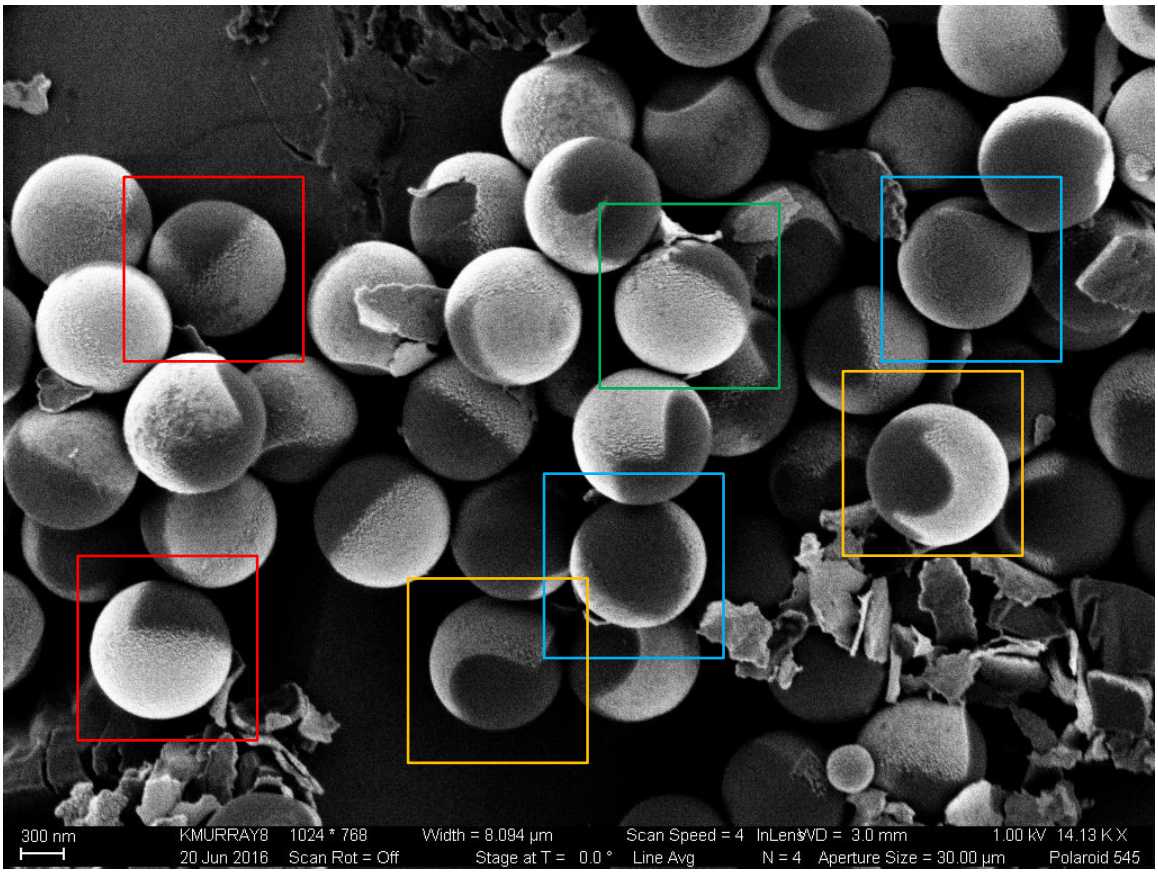

Figure 4-3. Multiple variable orientations of multi-region particles. Red boxes identify particles with a side orientation in which all three regions can be seen and the angle of deposition can be verified. Blue regions show particles in which only the base particle can be seen. Green boxes show particles in which only one metal region can be seen. Yellow boxes show evidence of shielding on particle metal evaporation coverage.

The final, optimized fabrication protocol is as follows: a 5 nm titanium sticking layer was evaporated onto the slides followed by a 30 nm gold layer at a rate of 3 Å/s. The slides were removed from the evaporator, rotated 90 degrees, and then returned to the evaporating chamber. 20 nm nickel at a rate of 3 Å/s was then evaporated onto the particles, creating orthogonally coated layers of gold and nickel.

The functionalization of the three-region Cerberus particles was optimized for order of conjugation, metal evaporation layer thickness, blocking agent, and protein concentration.

From the results in Figure 3-3 and 3-4, flow cytometry data showed the signal from each of the three sides on the trifunctional particle was distinguishable from the negative control. Compared to the single positive controls, the trifunctional was not as bright, however this could have been due to signal interference. Compensation was used during flow cytometry to reduce this. Additionally, there could have been more non-specific adsorption in the single controls without the other proteins present.

In optimizing the functionalization for spatial segregation, Figure 3-5 compared two protocols. Protocol 1 involves functionalization of the gold region first with thiol-PEG-biotin, then the silica side with APTES/IgG. SA (gold) and HIS-GFP (nickel) are added last. Protocol 2 involved functionalization of the silica side with APTES/IgG, followed by the gold side with thiol-PEG-biotin and SA and the HIS-GFP functionalization last. Since APTES is a harsh chemical, proteins would most likely denature if already conjugated to the particle. TPB is a very stable linker molecule which can withstand the harsh conditions required by the APTES treatment. In addition, the IgG conjugation must always follow the APTES silanization of the silica as the treatment allows for passive adsorption. The interaction between SA and biotin is one of the strongest known in nature and this allows for the SA to be conjugated after the APTES/IgG conjugation. However, we also see from the fluorescent images, that there is a noticeable amount of non-specific binding in the single controls and even in the trifunctional group. While blocking was used prior to antibody staining, any blocking attempted before or during conjugation resulted in no functionalization of any side. All three of the proteins used in this study have some non-specific binding despite the specific conjugation schemes used for each metal region.

Quantification of spatial segregation was not performed as there is not a well-established method, similarly for the verification of the glancing angle metal evaporation fabrication. In the 3D renderings of the trifunctionalized particles in Figure 3-12, there are regions which have only IgG, GFP, or SA (blue/green/yellow). There are regions with multiple proteins (white), however there is an increase in spatial segregation. Additionally, there are many orientations of the particles which make visualization of the spatial segregation and the 3 regions difficult for an individual from. Of the particles analysed, on average, each particle had signal from all proteins with regions of only one protein as well as regions with no protein at all.

In examination of two control groups for conjugation specificity, gold Janus particles and nickel Janus particles, the thiol-PEG-biotin/SA and APTES/IgG were fairly specific to gold and silica, respectively (Appendix Figure A-2 and A3). There some overlap between the SA and IgG signal on the gold Janus particles (white regions) however it is clear there are two regions thus spatial segregation of the proteins. While we expected this result to occur with the nickel Janus particles and spatial segregation of the IgG and HIS-GFP, there was more overlap. There was also a noticeable reduction in signal on the nickel side. The IgG is spatially limited to the silica region of the particle but is overlapped with the gree HIS-GFP signal. Additionally, there is signal of the HIS-GFP on the nickel region compared to the negative control, however there is more protein on the silica side. While the histidine-nickel conjugation chemistry is well characterized[36,37,38,39,40], there are additional interactions occurring which do not allow for the complete spatial segregation of these proteins. It is not believed that there is non-specific antibody staining occurring based on the IgG only control and negative control which were subjected to primary

antibody against GFP. In order to increase spatial segregation and specificity of the HIS-tagged protein binding, it is recommended that alternate proteins be examined instead of IgG or an alternate base material be used for the particles. There is evidence that histidine interacts with silica and is involved in biosilification that may cause the increase in binding of the HIS-GFP to the silica region[41,42].

CHAPTER 5 CONCLUSION

5.1 Conclusion

The work in this thesis has developed a fabrication methodology to create a three-region Cerberus particle and a functionalization protocol to conjugate three proteins to each region with spatial segregation. Using metal evaporation at two distinct angles of deposition allows for the consistent and even fabrication of metal layers. While gold and nickel were the main metals of interest in this thesis, there are many other metals available which can be used to make Cerberus particles. Copper, platinum, iron, and silver are a few possible metals, each of which have well established conjugation chemistries associated with them to bind biological ligands or non-biological functionalities such as the ability to act as catalysts or magnets.

This thesis also begins to explore a few applications for trifunctional Cerberus particles. Using nickel's inherent magnetic property, this can allow for highly specific control of particles. We have shown that we can manipulate these particles with forward motion and rotational motion.

5.2 Future Work

Based on the results of the fabrication and functionalization of Cerberus particles, there is still much improvement to be done in order to increase spatial segregation. The proteins used to functionalize the particles, IgG, SA, and GFP, all displayed some non-specific interactions with other regions of the particle, indicating promiscuity of the binding

abilities of those proteins. Exploring other ligands of different sizes, charges, and tertiary structure could improve the specificity and spatial segregation of the binding.

There are also other conjugation schemes available for the metals used in this thesis which may improve the spatial segregation of the proteins. For silica functionalization, there are many protocols which functionalize silica wafers using a combination of APTES and NHS/EDS prior to passive adsorption[43,44,45,46]. For the nickel conjugation, there are methods which first conjugate a NTA-Ni surface layer prior to HIS tag protein functionalization. While this would not work directly with the metal evaporation process presented, it is an option which would increase binding ability of HIS tagged protein. Finally, for the gold conjugation, there are other functional thiols[47] or thiol-functionalized biological ligands which could be used instead of TPB. Binding density should be evaluated as the PEG linker creates more space for bulkier protein to bind.

In moving this work to become a translatable therapeutic, the size of the particle must be reduced into the nanometer range. As shown in the diameter to evaporation layer ratio optimization, 150 nm silica particles can be processed in the same manner to create three regions on the surface of the particle. From the SEM analysis, the metal evaporation is uneven and thick at the smaller scale. This could be improved by inducing a higher vacuum prior to deposition, depositing at a slower deposition rate, and reducing the thickness of the metal layer.

Another avenue for future applications of functionalized, spatially segregated Cerberus particles is the collection of secreted proteins from mesenchymal stem cells (MSCs). Extracellular communication is incredibly important in understanding how MSCs

affect the cells around them and control growth rates. The use of Cerberus particles conjugated with antibodies allow the study of the proteomics within only a few microns from the cell of choice. MSCs have angiogenic, inflammatory and matrix remodeling potential properties. These abilities should be further characterized in order to direct the best protocols for their therapeutic use. There is a key difference in the proteins MSCs secrete, depending on what they will differentiate into. This suggests there are effectors that cause the differentiation that could be detected prior to the beginning of the differentiation process.

As a preliminary study, we conjugated plain silica particles with anti-CD44 antibodies and evaluated the binding ability of the anti-CD44 coated particles. CD44 is a highly expressed surface protein on MSCs. From flow cytometry and fluorescent imaging, we can successfully conjugate CD44 to silica particles through APTES activation and CD44 conjugation (Figure 5-1).

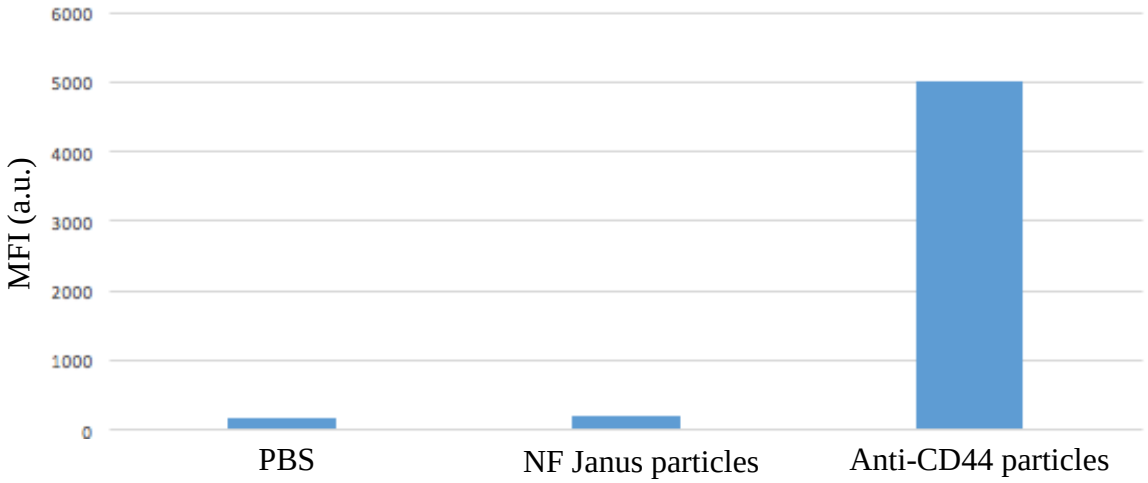

Figure 5-1. Janus particles can be functionalized with anti-CD44 antibody. Flow cytometry data of particles conjugated with FITC-labeled anti-CD44 has a higher fluorescence intensity compared to PBS with no particles and non-functionalized (NF) particles.

The functionalized anti-CD44 particles were then incubated with MSCs for 1 hour and analyzed with flow cytometry and fluorescent imaging. Both methods indicated positive binding of the particles to the cells (Figure 5-2). The ratio of particles to cells can be further optimized for increased binding. Additionally, we saw positive signal in the cells only control however there was a distinct negative cell population in the test sample (rightmost image in Figure 5-2 A). Further studies should be performed to further evaluate the binding capability of anti-CD44 conjugated particles.

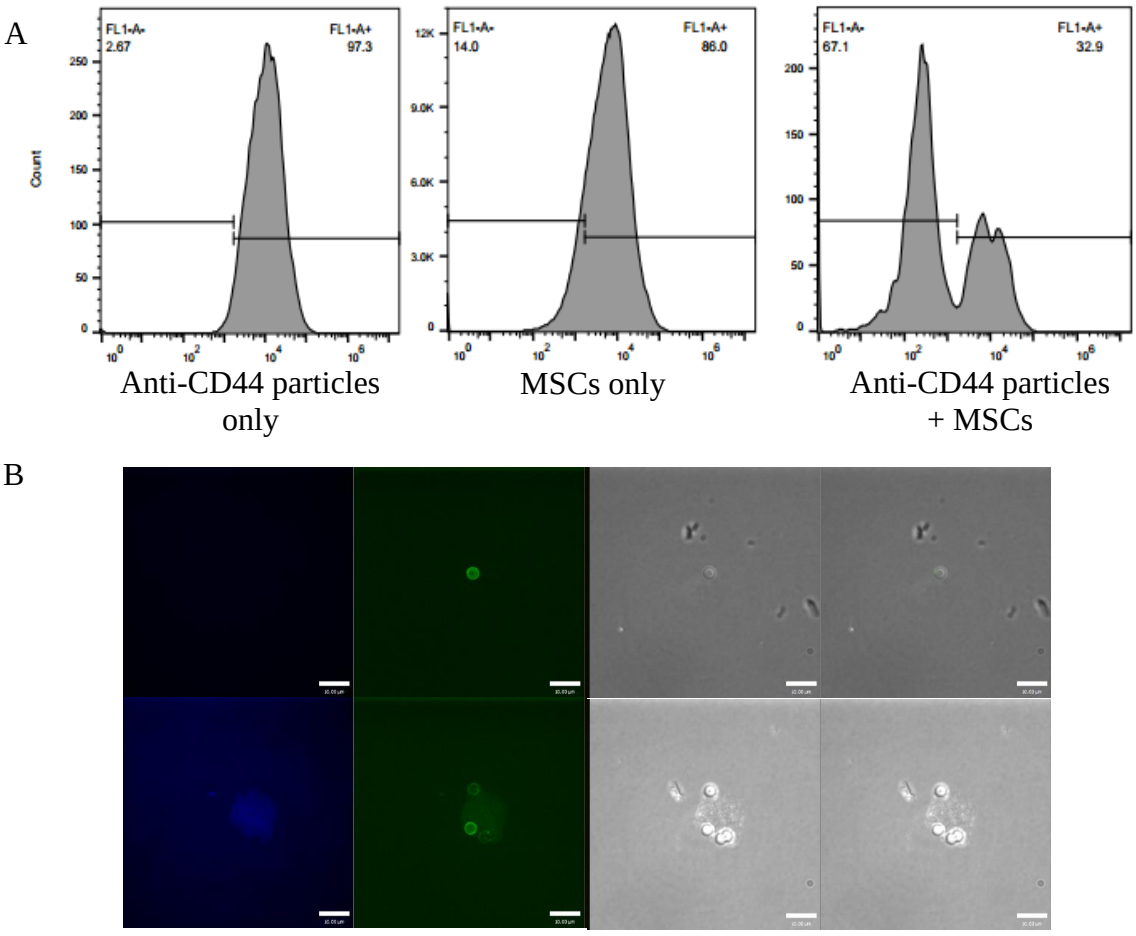

Figure 5-2. Anti-CD44 coated silica particles binds MSCs. (A) Flow cytometry data of MSCs incubated with anti-CD44 coated Janus particles. (B) Fluorescent images of anti-CD44 particles only (top) and anti-CD44 particles conjugated to a MSC. Scale bars are 10 μm.

The long-term goal of binding anti-CD44 coated particles to MSCs is to create Cerberus particles with one side targeted to MSCs with anti-CD44, and the other two sides with antibodies or ligands which can collect secreted antibodies from the specific MSC the particle is bound to. Two secreted proteins of interest include IL6 and VEGF as they are important for cell signaling and growth. The Cerberus particles can be conjugated with anti-IL6 and anti-VEGF antibodies to collect the corresponding secreted proteins. The development of a particle to collect secreted proteins can allow for further understanding of MSCs and their development as therapies.

In conclusion, this thesis has shown that repeated glancing angle metal evaporation can produce multi-region particles of different metals which can be functionalized based on specific chemical conjugation schemes. This fabrication is repeatable, customizable, and can be scaled down to nanoparticle size for future therapeutic applications. This work provides a new paradigm for the fabrication and functionalization for multifunctional particles.

APPENDIX A

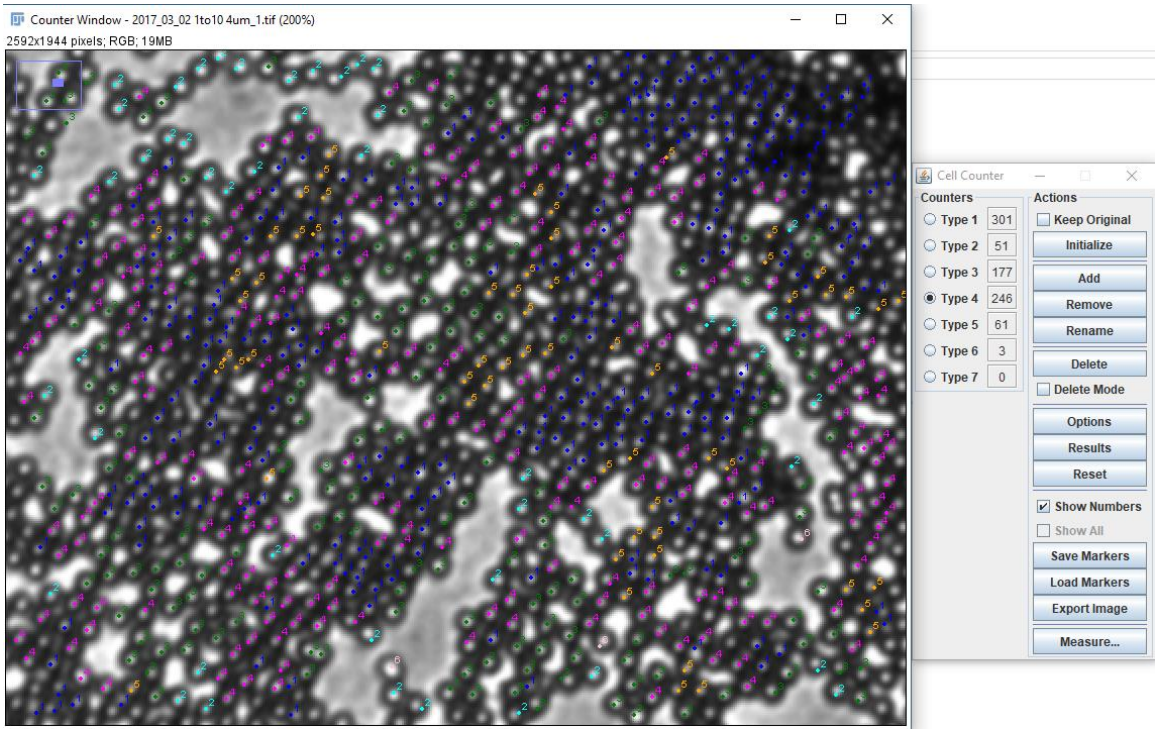

Figure A-1. Sample dispersity analysis of particles. Particle were counted based on how many neighbor particles it was touching.

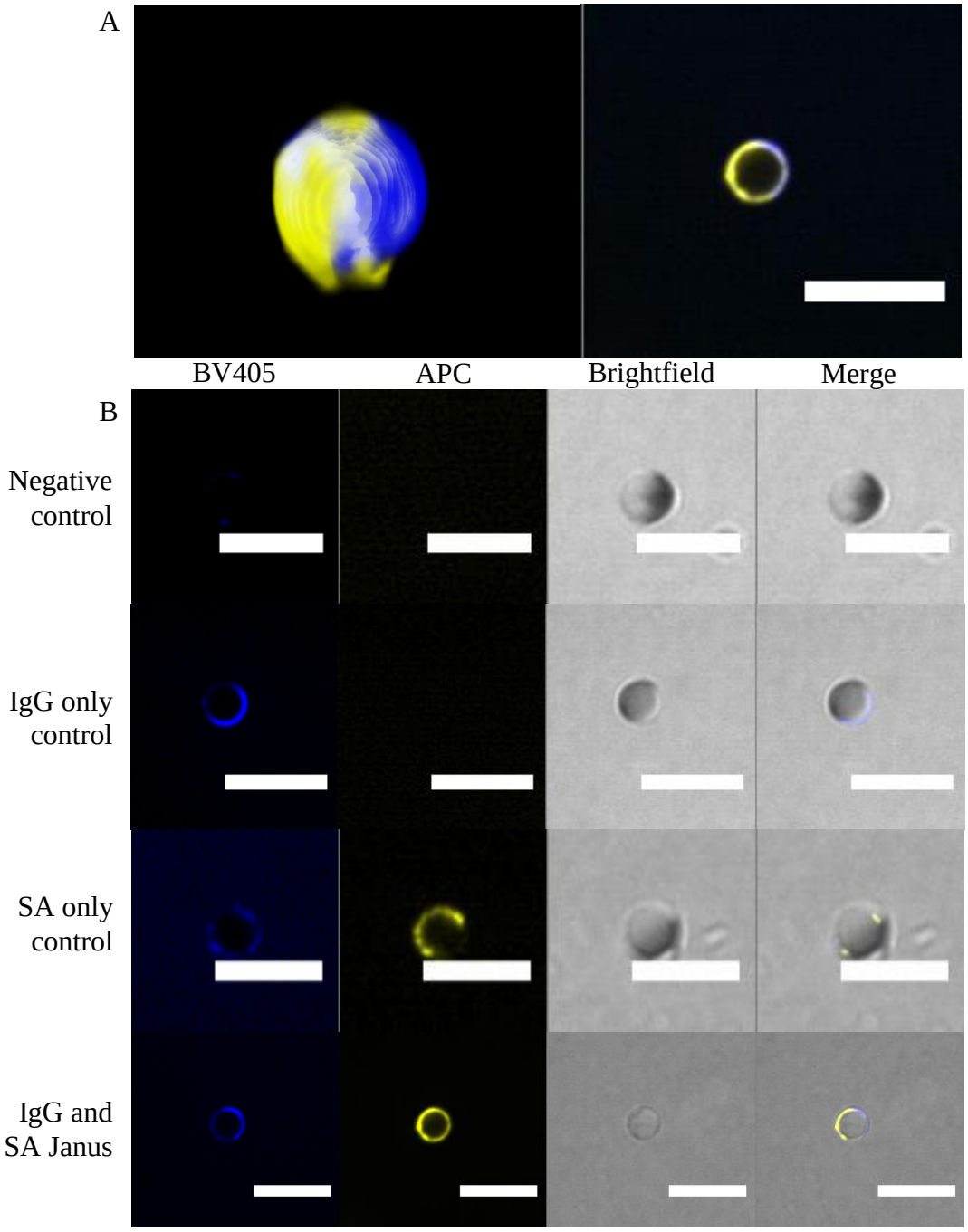

Figure A-2. Janus particles of gold and silica functionalized with SA and IgG are specific to the conjugations for each region. (A) 3D and 2D views of gold Janus particles with IgG (blue) and SA (yellow). (B) Single protein controls and trifunctional particles with IgG labeled with AlexaFluor 405 (blue), SA labeled in APC (yellow), and GFP labeled in FITC (green). Spatial segregation can be observed. Scale bars are 10 μm.

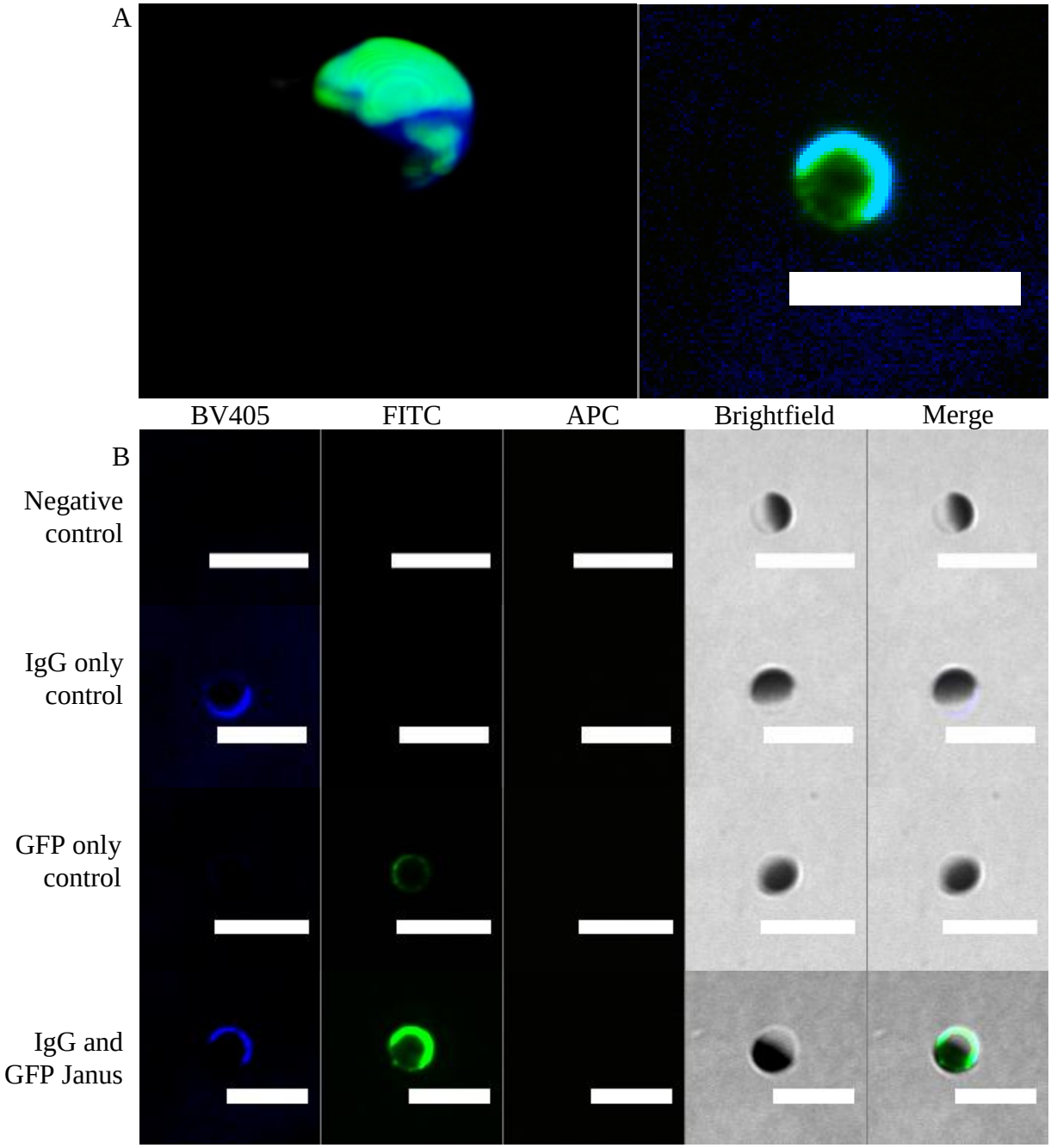

Figure A-3. Janus particles of nickel and silica are functionalized with HIS-GFP and IgG. (A) 3D and 2D views of nickel Janus particles with HIS-GFP (green) and IgG (blue). (B) Single protein controls and trifunctional particles with IgG labeled with AlexaFluor 405 (blue), SA labeled in APC (yellow), and GFP labeled in FITC (green). Scale bars are 10 μm.

REFERENCES

1. Bhaskar S, Pollock KM, Yoshida M, Lahann J. Towards designer microparticles: simultaneous control of anisotropv, shape and size. *Small*. 2010;6(3):404-411. doi:10.1002/smll.200901306.
2. Yi Y, Sanchez L, Gao Y, Lee K, Yu Y. Interrogating Cellular Functions with Designer Janus Particles. *Chem Mater*. 2017:acs.chemmater.6b05322. doi:10.1021/acs.chemmater.6b05322.
3. Pensa E, Cortés E, Corthey G, et al. The chemistry of the sulfur-gold interface: In search of a unified model. *Acc Chem Res*. 2012;45(8):1183-1192. doi:10.1021/ar200260p.
4. Kwon H-S, Jung S-G, Kim H-Y, Parker S a., Batt C a., Kim Y-R. A multi-functional polyhydroxybutyrate nanoparticle for theranostic applications. *J Mater Chem B*. 2014;2(25):3965. doi:10.1039/c4tb00304g.
5. Reguera J, Aberasturi DJ De, Henriksen-lacey M, et al. Janus plasmonic–magnetic gold–iron oxide nanoparticles as contrast agents for multimodal imaging. 2017. doi:10.1039/c7nr01406f.
6. Perica K, Tu A, Richter A, Bieler JG, Edidin M, Schneck JP. Magnetic field-induced t cell receptor clustering by nanoparticles enhances t cell activation and stimulates antitumor activity. *ACS Nano*. 2014;8(3):2252-2260. doi:10.1021/nn405520d.
7. Cho KJ, Wang X, Nie SM, Chen Z, Shin DM. Therapeutic nanoparticles for drug delivery in cancer. *Clin CANCER Res*. 2008;14(5):1310-1316. http://prx.library.gatech.edu/login?url=https://search.ebscohost.com/login.aspx?direct=true&db=edswsc&AN=000253565000007&site=eds-live&scope=site.
8. Rahmani S, Lahann J. Recent progress with multicompartmental nanoparticles. *MRS Bull*. 2014;39(3):251-257. doi:10.1557/mrs.2014.10.
9. Bhaskar S, Tian F, Stoeger T, et al. Multifunctional Nanocarriers for diagnostics, drug delivery and targeted treatment across blood-brain barrier: perspectives on tracking and neuroimaging. *Part Fibre Toxicol*. 2010;7:3. doi:10.1186/1743-8977-7-3.
10. Sun XT, Liu M, Xu ZR. Microfluidic fabrication of multifunctional particles and their analytical applications. *Talanta*. 2014;121:163-177. doi:10.1016/j.talanta.2013.12.060.
11. He F, Wang W, He X-H, et al. Controllable Multi-Compartmental Capsules with Distinct Cores and Shells for Synergistic Release. *ACS Appl Mater Interfaces*. 2016. doi:10.1021/acsami.6b01278.
12. Zhao Y, Cheng Y, Shang L, Wang J, Xie Z, Gu Z. Microfluidic synthesis of barcode particles for multiplex assays. *Small*. 2015;11(2):151-174. doi:10.1002/smll.201401600.
13. Yi Y, Sanchez L, Gao Y, Yu Y. Janus particles for biological imaging and sensing. *Analyst*. 2016:3526-3539. doi:10.1039/c6an00325g.
14. Rahmani S, Saha S, Durmaz H, et al. Chemically Orthogonal Three-Patch Microparticles. *Angew CHEMIE-INTERNATIONAL Ed*. 2014;53(9):2332-2338. doi:10.1002/anie.201310727.

15. Cho K, Lee HJ, Han SW, Min JH, Park H, Koh WG. Multi-Compartmental Hydrogel Microparticles Fabricated by Combination of Sequential Electrospinning and Photopatterning. *Angew Chemie - Int Ed*. 2015;54(39):11511-11515. doi:10.1002/anie.201504317.
16. Fan L, Zhang Y, Wang F, et al. Multifunctional all-in-one drug delivery systems for tumor targeting and sequential release of three different anti-tumor drugs. *Biomaterials*. 2016;76:399-407. 10.1016/j.biomaterials.2015.10.069.
17. Kumar S, Aaron J, Sokolov K. Directional conjugation of antibodies to nanoparticles for synthesis of multiplexed optical contrast agents with both delivery and targeting moieties. *Nat Protoc*. 2008;3(2):314-320. doi:10.1038/nprot.2008.1.
18. Yoon JH, Kim DK, Na M, Lee SY. Multi-ligand functionalized particle design for cell targeting and drug delivery. *Biophys Chem*. 2016;213:25-31. doi:10.1016/j.bpc.2016.03.006.
19. Kim J(1), Lee JE(1), Lee J(1), et al. Generalized fabrication of multifunctional nanoparticle assemblies on silica spheres. *Angew Chemie - Int Ed*. 2006;45(29):4789-4793. doi:10.1002/anie.200504107.
20. Liu J, Wei T, Zhao J, et al. Multifunctional aptamer-based nanoparticles for targeted drug delivery to circumvent cancer resistance. *Biomaterials*. 2016;91:44-56. doi:10.1016/j.biomaterials.2016.03.013.
21. Rizk N, Christoforou N, Lee S. Optimization of anti-cancer drugs and a targeting molecule on multifunctional gold nanoparticles. *Nanotechnology*. 2016;27(18):185704. doi:10.1088/0957-4484/27/18/185704.
22. Kim K, Oh KS, Park DY, et al. Doxorubicin/gold-loaded core/shell nanoparticles for combination therapy to treat cancer through the enhanced tumor targeting. *J Control Release*. 2016;228:141-149. doi:10.1016/j.jconrel.2016.03.009.
23. Hayakawa M, Onoe H, Nagai KH, Takinoue M. Complex-shaped three-dimensional multi-compartmental microparticles generated by diffusional and Marangoni microflows in centrifugally discharged droplets. *Sci Rep*. 2016;6(February):20793. doi:10.1038/srep20793.
24. Kaewsaneha C, Tangboriboonrat P, Polpanich D, Eissa M, Elaissari A. Preparation of Janus colloidal particles via Pickering emulsion: An overview. *Colloids Surfaces A Physicochem Eng Asp*. 2013;439:35-42. doi:10.1016/j.colsurfa.2013.01.004.
25. Khan IU, Serra CA, Anton N, et al. Microfluidic conceived drug loaded Janus particles in side-by-side capillaries device. *Int J Pharm*. 2014;473(1/2):239-249. 10.1016/j.ijpharm.2014.06.035.
26. Chen P-C. Polyelemental nanoparticle libraries. *Nanomaterials*. 2016;352(6293):1565-1570.
27. Tang JL, Schoenwald K, Potter D, White D, Sulchek T. Bifunctional janus microparticles with spatially segregated proteins. *Langmuir*. 2012;28(26):10033-10039. doi:10.1021/la3010079.
28. Sperling RA, Rivera Gil P, Zhang F, Zanella M, Parak WJ. Biological applications of gold nanoparticles. *Chem Soc Rev*. 2008;37(9):1896-1908. doi:10.1039/B712170A.
29. Subramanian G, ed. *Biopharmaceutical Production Technology*. John Wiley & Sons, Incorporated; 2012. http://ebookcentral.proquest.com.prx.library.gatech.edu/lib/gatech/detail.action?do

cID=922193.
30. McNaughton BH, Vladimir S, Anker JN, Roy C, Kopelman R. Fabrication of uniform half-shell magnetic nanoparticles and microspheres with applications as magnetically modulated optical nanoprobes. *System*. 2005;33(0):1-23.
31. Lee KB, Park S, Mirkin CA. Multicomponent magnetic nanorods for biomolecular separations. *Angew Chemie - Int Ed*. 2004;43(23):3048-3050. doi:10.1002/anie.200454088.
32. Lee K, Yi Y, Yu Y. Remote Control of T Cell Activation Using Magnetic Janus Particles. *Angew Chemie Int Ed*. 2016:1-5. doi:10.1002/anie.201601211.
33. Kurihara Y, Hosokawa T, Saitoh R. The influence of interdiffusion of metals in an evaporated multilayer metallization on the adhesion of an Sn-Sb solder.pdf. *Electron Commun Japan*. 1995;78(7).
34. Martin PJ, Bendavid A, Comte C, et al. Alignment and switching behaviors of liquid crystal on a-SiO[sub x] thin films deposited by a filtered cathodic arc process. *Appl Phys Lett*. 2007;91(6):63516. doi:10.1063/1.2768308.
35. Zeeshan M a, Shou K, Pané S, et al. Structural and magnetic characterization of batch-fabricated nickel encapsulated multi-walled carbon nanotubes. *Nanotechnology*. 2011;22(27):275713. doi:10.1088/0957-4484/22/27/275713.
36. Agarwal G, Naik RR, Stone MO, Base WAF, Management T. Immobilization of Histidine-Tagged Proteins on Nickel by Electrochemical Dip Pen Nanolithography potentially important prerequisite for the fabrication of biosen-. *Am Chem Soc*. 2003;(15):7408-7412.
37. Liu Z, Li M, Li Z, Pu F, Ren J, Qu X. Easy Access to Selective Binding and Recyclable Separation of Histidine-Tagged Proteins Using Ni 2 + -Decorated Superparamag- netic Nanoparticles. *Nano Res*. 2012;5(7):450-459. doi:10.1007/s12274-012-0230-5.
38. Patel JD, O'Carra R, Jones J, Woodward JG, Mumper RJ. Preparation and characterization of nickel nanoparticles for binding to his-tag proteins and antigens. *Pharm Res*. 2007;24(2):343-352. doi:10.1007/s11095-006-9154-7.
39. Nam JM, Han SW, Lee KB, Liu X, Ratner MA, Mirkin CA. Bioactive protein nanoarrays on nickel oxide surfaces formed by dip-pen nanolithography. *Angew Chemie - Int Ed*. 2004;43(10):1246-1249. doi:10.1002/anie.200353203.
40. Bodelón G, Mourdikoudis S, Yate L, Pastoriza-Santos I, Pérez-Juste J, Liz-Marzán LM. Nickel nanoparticle-doped paper as a bioactive scaffold for targeted and robust immobilization of functional proteins. *ACS Nano*. 2014;8(6):6221-6231. doi:10.1021/nn5016665.
41. Gao X, Li Y, Qin Y, et al. Reversible and oriented immobilization of histidine-tagged protein on silica gel characterized by frontal analysis. *RSC Adv*. 2015;5(31):24449-24454. doi:10.1039/C5RA01012H.
42. Kubota LT, Gambero A, Santos AS, Granjeiro JM. Study of the Adsorption of Some Amino Acids by Silica Chemically Modified with Aminobenzenesulfonic and Phosphate Groups. *J Colloid Interface Sci*. 1996;183(2):453-457. doi:10.1006/jcis.1996.0568.
43. Landoulsi J, Genet MJ, Kirat K El, Richard C, Pulvin S, Rouxhe PG. Silanization with APTES for Controlling the Interactions Between Stainless Steel and Biocomponents: Reality vs Expectation. *Biomater - Phys Chem*. 2011;5:99-126.

doi:978-953-307-418-4.
44. Kim J, Cho J, Seidler PM, Kurland NE, Yadavalli VK. Investigations of chemical modifications of amino-terminated organic films on silicon substrates and controlled protein immobilization. *Langmuir*. 2010;26(4):2599-2608. doi:10.1021/la904027p.
45. Torati SR, Reddy V, Yoon SS, Kim CG. Protein immobilization onto electrochemically synthesized CoFe nanowires. *Int J Nanomedicine*. 2015;10:645-651. doi:10.2147/IJN.S76850.
46. Acres RG, Ellis A V., Alvino J, et al. Molecular structure of 3-aminopropyltriethoxysilane layers formed on silanol-terminated silicon surfaces. *J Phys Chem C*. 2012;116(10):6289-6297. doi:10.1021/jp212056s.
47. Kaufmann T, Wendeln C, Gokmen MT, et al. Chemically orthogonal trifunctional Janus beads by photochemical "sandwich" microcontact printing. *Chem Commun (Camb)*. 2013;49(1):63-65. doi:10.1039/c2cc36483b.